

126

**ELECTRON PARAMAGNETIC RESONANCE
OF Cr^{3+}
IN GUANIDINIUM ALUMINUM SULFATE HEXAHYDRATE**

Pierre Giguère

**A THESIS
in
The Department
of
Physics**

**Presented in Partial Fulfillment of the Requirements
for the Degree of Master of Science
at Concordia University
Montreal, Quebec, Canada**

September, 1976

ABSTRACT

PIERRE GIGUERE

ELECTRON PARAMAGNETIC RESONANCE OF Cr^{3+}
IN GUANIDINIUM ALUMINUM SULFATE HEXAHYDRATE

A paramagnetic resonance study of Cr^{3+} substituted for aluminum in guanidinium aluminum sulfate hexahydrate (GASH), made at X-band frequencies is reported. The chromium ion in GASH features many interesting properties which stimulate its study and make it pedagogically valuable: simple spectra easily fitted by an Hamiltonian, existence of two sets of lines due to two non equivalent sites, spectra easily obtained at all angles and all temperatures, appearance of relatively strong $|\Delta M| = 2$, $|\Delta M| = 3$ transition lines.

Our original contribution will be the calculated values of the spin Hamiltonian parameters at liquid helium temperature, and also the absolute sign of the D parameter.

At 1,61 K, we find for the first site (the more populated)
 $g_{zz} = 1,987 \pm ,003$, $g_{xx} = g_{yy} = 1,985 \pm ,003$, $D = -2,677 \pm ,008$ GHz;
for the second site (the less populated) we find $g_{zz} = 1,984 \pm ,003$,
 $g_{xx} = g_{yy} = 1,985 \pm ,003$, $D = -3,492 \pm ,008$ GHz.

ACKNOWLEDGEMENTS

The author wishes to express gratitude to Dr. S.K. Miers for proposing this work and for his continued interest, encouragement and advice. He gratefully acknowledges the assistance of his fellow graduate student G.R. Sharp for training and advice on the spectrometer whose development has been his Master of Science thesis project. He is also grateful for the encouragement and motivation provided by parents and friends, specially Miss Andrée Ste-Marie who also typed the thesis.

The importance of all these relations on the completion of a thesis by a part time student, professionally and socially engaged, cannot be overestimated.

This work has profited from Professor Miers's N.R.C. grants

TABLE OF CONTENTS

Abstract	1
Acknowledgements	11
I. INTRODUCTION	1
II. THEORY	2
2.1 Historical Survey	2
2.2 The Spin Hamiltonian and the Conditions of Transition	3
2.3 Fitting the Hamiltonian to a Given Spectrum	9
III. EXPERIMENTAL PROCEDURE	12
3.1 Crystal Structure and Sample Preparation	12
3.2 The Paramagnetic Resonance Spectrometer	15
3.3 Production of the Spectra	23
3.4 Measurement of the Resonant Field Values	25
IV. DATA AND ANALYSIS	27
4.1 At Room Temperature	27
4.2 At Liquid Nitrogen Temperature	34
4.3 At Liquid Helium Temperature	39
V. CONCLUSION	47
Appendix	48
Bibliography	67

CHAPTER I

INTRODUCTION

We report an electron paramagnetic resonance (EPR) study of Cr^{3+} in guanidinium aluminum sulfate hexahydrate, $\text{C}(\text{NH}_2)_3 \cdot \text{Al}(\text{SO}_4)_2 \cdot 6 \text{H}_2\text{O}$; we present quantitative results where results published previously were qualitative.

Chapter II shows the historical development of the EPR field with particular attention on past studies of ions in GASH or similar salts; that chapter also reviews the theoretical formalism used to interpret the EPR spectra, i.e. the spin Hamiltonian, and also the numerical procedure we used to extract the values of the parameters.

The experimental procedure is the subject of chapter III.

The data obtained at three different temperatures, room temperature, liquid nitrogen temperature, and liquid helium temperature, and their analysis are presented in chapter IV.

CHAPTER II

THEORY

2.1 Historical Survey

The evolution of electron spin resonance begins with the discovery of the phenomena by Zavoisky¹ in 1945. He observed strong paramagnetic resonance absorptions in several salts; in his first experiment he detected a peak in the paramagnetic absorption from $\text{CuCl}_2 \cdot 2\text{H}_2\text{O}$. Other early contributors to the field were Bleaney and Penrose².

In the past thirty years this field has grown tremendously and has been the subject of a large number of publications.

In particular, the interesting ferroelectric GASH has been extensively used as the non magnetic host to study the electronic structure of transition metal ions in crystals^{3,4,5,6}.

The interest in GASH and its isomorphs dates back to 1955^{7,8}; the easy growing from aqueous solution, the three aluminum ions per unit cell, two of which are equivalent, the ferroelectric property demonstrated at all temperatures consistent with the crystalline state, the space group C_{3v} for a ferroelectric crystal were all interesting facets of this new class of salts.

In 1957, Bogle⁹ reported the first EPR study of Cr^{3+} substituted in GASH, which at the time was the only ferroelectric salt containing a paramagnetic ion that could be crystallized from aqueous solution.

Using DPPH as a marker, Bogle studied the crystal at 17 K and 100 K, disclosing two independent spectra, one twice as intense as the other, both with the same symmetry axis, coinciding with the three-fold crystal axis; the g tensor was found to be isotropic.

More recent studies^{3,5} have repeated his results and extended them qualitatively at liquid helium temperature.

2.2 The Spin Hamiltonian and the Conditions of Transition

The Cr atom has a ground state configuration of $4s3d^5$; although its chemical properties are mostly related to its outermost electron, as well as for other transition metal ions, it is the electrons of the incomplete 3d shell which are responsible for its interesting magnetic properties; in fact, of the $3d^3$ ions, Cr^{3+} and its complexes have been studied more than any other ions¹⁰.

Transition metal ions have a non zero total angular momentum. Substitution in low concentration of transition metal ions into a diamagnetic substance creates a paramagnetic substance; the transi-

tion metal, rare-earth, and actinide ions have so been the subject of a host of EPR investigations.

When a paramagnetic substance is placed in a steady magnetic field, Zeeman splitting of the energy levels occurs and photons having energies equal to the gaps between the Zeeman levels may induce transitions. The energy absorbed as a function of magnetic field strength is referred to as the paramagnetic resonance spectrum of the substance ¹⁰.

However, when ions are placed in condensed media, the interaction of the ions with the electric field of their neighbours alters the array of energy levels.

The electronic interactions which contribute to the total energy of the ion can be represented by the following spin Hamiltonian ¹¹:

$$\mathcal{H} = \mathcal{H}_{\text{elec}} + \mathcal{H}_{\text{cf}} + \mathcal{H}_{\text{LS}} + \mathcal{H}_{\text{SS}} + \mathcal{H}_{\text{Zee}} + \mathcal{H}_{\text{hfs}} + \mathcal{H}_{\text{Q}} + \mathcal{H}_{\text{N}}$$

or in terms of spin operators O_k^q ¹²,

$$\mathcal{H} = \mathcal{H}_{\text{Zee}} + \sum_{\substack{k,q \\ q \leq k}} B_k^q O_k^q$$

where the spin operators are limited by the symmetries of the crystal field and restricted to even degrees, since odd degree operators are not invariant under time reversal.

Table 1 gives the typical form of each term and their magnitudes.

Table 1. The various terms of the spin Hamiltonian

$\mathcal{H}_{\text{elect}}$	= electronic energy = $10^4 - 10^5 \text{ cm}^{-1}$ (optical region)
\mathcal{H}_{cf}	= crystal field energy = $10^3 - 10^4 \text{ cm}^{-1}$ (infrared or optical region)
\mathcal{H}_{LS}	= spin orbit interaction = $10^2 \text{ cm}^{-1} = \lambda \bar{L} \cdot \bar{S}$
\mathcal{H}_{SS}	= spin-spin interaction = $0 - 1 \text{ cm}^{-1} = D(S_z^2 - S(S+1)/3)$
\mathcal{H}_{Zee}	= Zeeman energy = $0 - 1 \text{ cm}^{-1} = \beta (\bar{H} \cdot \bar{g} \cdot \bar{S})$
\mathcal{H}_{hfs}	= hyperfine structure = $0 - 10^{-2} \text{ cm}^{-1} = (\bar{S} \cdot \bar{A} \cdot \bar{I})$
\mathcal{H}_{Q}	= quadrupole energy = $0 - 10^{-2} \text{ cm}^{-1}$ $= \left\{ \frac{3 e Q}{4I(2I-1)} \right\} \times \frac{\partial^2 V}{\partial z^2} \left[\frac{I_z^2}{I(I+1)} - \frac{I(I+1)}{3} \right]$
\mathcal{H}_{N}	= nuclear spin energy = $0 - 10^{-3} \text{ cm}^{-1} = (\bar{H} \cdot \bar{I}) \gamma \beta_n$

The symbols have the following meaning:

- λ , spin orbit coupling constant
- S , electronic spin
- L , orbital quantum number
- D , zero field splitting constant

- β , Bohr magneton
- β_n , nuclear magneton
- e , electronic charge
- γ , nuclear magnetogyric ratio
- A , hyperfine coupling tensor
- I , nuclear spin
- Q , nuclear quadrupole moment
- V , crystalline electric field potential
- H , magnetic field
- g , g tensor

Since the energy contribution from the various terms ranges over nine decades, some of the interactions fall out of the realm of EPR. The terms $\mathcal{H}_{\text{elect}}$, \mathcal{H}_{cf} , and \mathcal{H}_{LS} involve too much energy for excitation, while the terms \mathcal{H}_Q and \mathcal{H}_N are too small to be observed in most cases.

So the Hamiltonian

$$\mathcal{H} = \mathcal{H}_{\text{ee}} + \mathcal{H}_{\text{SS}} + \mathcal{H}_{\text{hfs}}$$

is sufficient in most cases.

For the Cr^{3+} ions, the ground state configuration being $3d^3$, along with Hund's rules ¹³,

$$S = 3/2$$

$$L = 3$$

$$J = 3/2,$$

their ground state is noted ⁴F 3/2.

But the degree of the spin operators in the Hamiltonian is limited to be $\leq 2S^2$.

So, theoretically, the most general Hamiltonian sufficient to describe ions with $S = 3/2$ is

$$\mathcal{H} = \mathcal{H}_{ZeS} + B_2^0 O_2^0 + B_2^2 O_2^2$$

or
$$\mathcal{H} = g(\vec{H} \cdot \vec{S}) + D (S_z^2 - S(S+1)/3) + 1/2 E (S_+^2 + S_-^2),$$

with $D = 3 B_2^0$ and $E = B_2^2$.

Moreover the C_{3v} crystal symmetry implies that the O_2^2 term of the Hamiltonian should not be used; in fact Bogle, Daniels and others have shown that for Cr^{3+} ions in GASH, the Hamiltonian

$$\mathcal{H} = g(\vec{H} \cdot \vec{S}) + D (S_z^2 - S(S+1)/3)$$

is sufficient to account for all the positions and variations of the lines of the EPR spectrum.

Since $S = 3/2$ for Cr^{3+} , the applied magnetic field will split the ground state level into four levels, corresponding to $M = -3/2, -1/2, 1/2, 3/2$.

Figure 1 shows these levels and the transitions or resonances

that could be induced by using the proper radio frequency magnetic field.

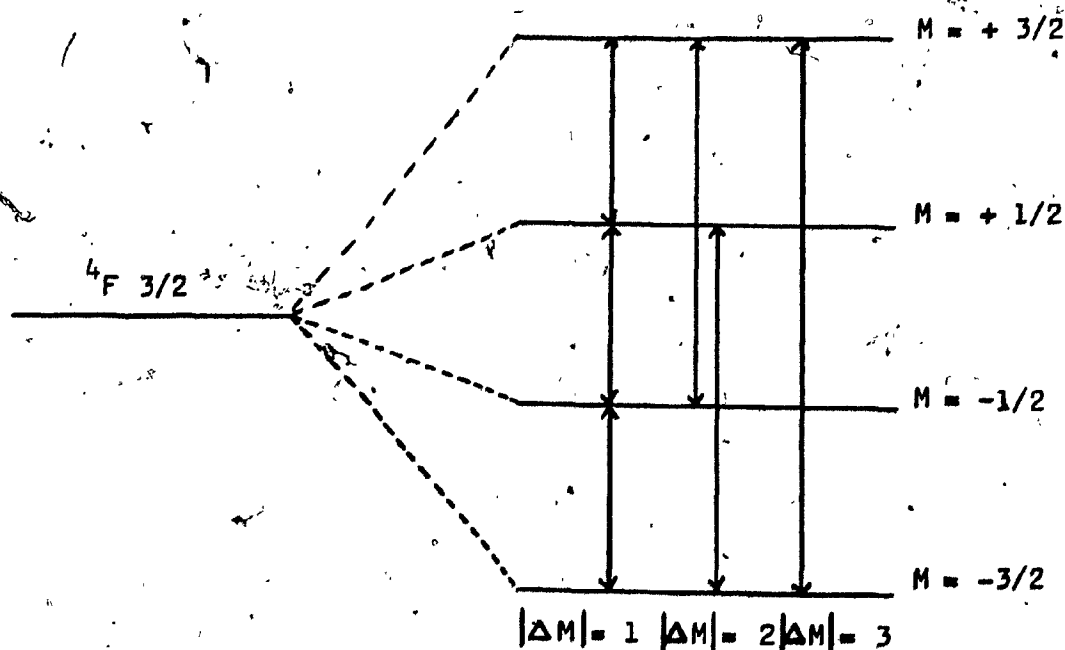


Fig. 1. Levels and transitions for Cr^{3+} in a magnetic field

The magnetic fields at which these transitions occur alter with the frequency of the applied radiation, and if anisotropy is present they will also depend on the orientation of the external magnetic field with respect to the crystal axes.

Clearly if in practice the r.f. field, maintained at a given frequency or energy, it is the variation of the applied magnetic field that will create the conditions necessary to produce all six different transitions.

The laboratory Z axis being chosen to coincide with the crystal C axis, the energy levels vary linearly with the applied magnetic field, when $H // Z$,

$$E_{\pm 1/2} = \pm \frac{1}{2} g \beta H - D$$

$$E_{\pm 3/2} = \pm \frac{3}{2} g \beta H + D.$$

In zero magnetic field there are pairs of degenerate energy levels at $\pm D$. These pairs, which reflect the Kramers degeneracy of an ion with an odd number of electrons, are called Kramers doublets.

2.3 Fitting the Hamiltonian to a given spectrum

Misra and Sharp¹⁴ developed an iterative "brute force" method of analysis of EPR data in which those parameters which have magnitudes of the same order are simultaneously varied over their chosen range. This method can handle the data corresponding to a spin Hamiltonian containing large off diagonal elements.

A quick, accurate procedure for the analysis using the least-squares fitting technique has been developed by Misra¹⁵. In this procedure one uses simultaneously field values obtained along any number of directions of the magnetic field with respect to the crystal axes, including transitions with $|\Delta M| \geq 1$.

The computer program for the analysis of our data using this procedure ¹⁵ is given in the appendix. It uses a simultaneous diagonalization of the Hamiltonian for field values obtained with the magnetic field along the Z axis, as well as for field values obtained with the magnetic field along the X axis.

In our case, we used as input data for each site, at each temperature:

- the value of magnetic field (in 10^4 gauss) for DPPH resonance giving indirectly the energy of the microwave field;
- the six values of the magnetic field (in 10^4 gauss) at the $|\Delta M| = 1$ transitions, three along the Z axis and three along the X axis;
- initial (trial) values for all the parameters; in our case we first used the values reported by Daniels and Wesemeyer ³ and values extrapolated from these at liquid helium temperature.

A series of synthetic transitions are constructed from the Hamiltonian and a least-squares criterion is employed to obtain a convergent sequence for determining the best-fit g values and crystalline electric field parameters; for each calculated spectrum, the mean square deviation (MSD) is determined using

$$BMD = \sum_j (|\Delta E_j| - h\nu)^2,$$

where ΔE_j is the energy difference between calculated levels participating in resonance at the j -th resonant field value, $h\nu$ is the energy of microwave radiation, and the index j covers all $|\Delta M| = 1$ lines.

Our final output data for a given site at a given temperature consisted of the values of g_{zz} , g_{xx} , B_2^0 and BMD.

As an example, in the case of the spectrum due to site I at liquid helium temperature, our input data consisted of the DPPH field value (3293), g_{zz} (1,986), g_{xx} (1,986), B_2^0 (-8922 GHz) and magnetic field values along z axis (in decreasing order) and along X axis (in increasing order) (5238; 3324; 1391; 2414; 3101; 4271); the output data consisted of g_{zz} (1,987), g_{xx} (1,986), B_2^0 (-8923 GHz), BMD (0,00096 GHz²); B_2^0 was then transformed into D by using $D = 3 B_2^0$.

CHAPTER III

EXPERIMENTAL PROCEDURE

3.1 Crystal Structure and Sample Preparation

The crystal structure of GASH has been determined by Geller and Booth^{16,17}. The space group of this trigonal crystal is $C_{3v}-P\bar{3}1m$ with three molecules per cell as shown in fig. 2.

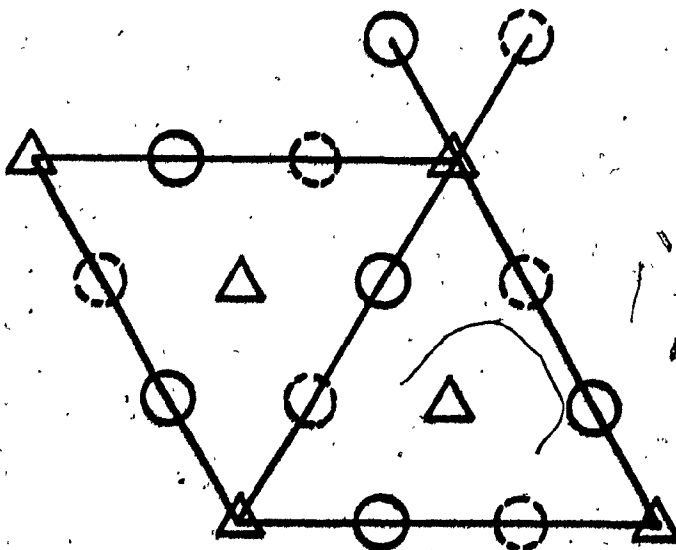


Fig.2 A schematic diagram of a unit cell of GASH looking down the C-axis.

The triangles represent threefold axes with Al ions in the plane of the paper and a guanidinium ion above and below. Each Al ion is octahedrally surrounded by six waters. The circles represent SO_4^{2-} groups above the plane and the dotted ones below.

The Al^{3+} ions (replaced by Cr^{3+} ions) are on threefold axes and are surrounded by a somewhat distorted octahedra of waters. The guanidinium ions are loosely bound indicating the possibility of disorder or rotation. Of the three Al ions per cell, two are equivalent to each other and are called to belong to site I; the other is called to belong to site II. In the EPR spectrum of Cr^{3+} in GASH this is equivalent to having two sets of lines superimposing each other, the intensities of the lines due to site I being twice of those due to site II. The unit cell parameters are $a = 11,738 \text{ \AA}^0$ and $c = 8,851 \text{ \AA}^0$; when Cr^{3+} is substituted in GASH, the dimensions of the unit cell are slightly increased ¹⁸.

The crystals were grown from an aqueous solution of calculated amounts of guanidinium sulfate, aluminum sulfate and chromium sulfate, the solution being made slightly acidic with sulfuric acid to prevent the hydrolysis of the chromium ion ⁴. The solution was allowed to evaporate slowly from a covered beaker. At first small platelets formed on the surface and sank to the bottom; these were then allowed to grow in place.

Different concentrations of chromium relative to aluminum have been studied; although they alter the shape of the lines, they produce the same overall spectrum and produce the same values of the parameters; the final concentration of chromium relative to aluminum in the crystals is most likely to be the same as the starting concentration in the aqueous solution (1% in the sample used for our measurements).

The crystals grow as hexagonal plates with normals accurately parallel to the crystal c axis, fig. 3.

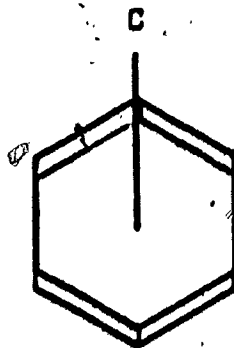


Fig. 3. Sketch of a single crystal of GASH, showing the relationship of the c axis to the external morphology.

The crystals had a light blue color; the higher the concentration of chromium in the crystals, the darker their blue color.

The crystals we used had linear dimensions of about, 5cm and a thickness of about, 1cm.

3.2 The Paramagnetic Resonance Spectrometer

A reflection cavity X-band spectrometer¹⁹ was used to obtain the spectra. A block diagram of the spectrometer is shown in fig. 4.

The microwave source is a forced air cooled Varian X-13 reflex klystron with a frequency range of 8,1 to 12,4 GHz and a power rating of 180 mw. A Hewlett Packard model 715 A power supply produces the required beam voltage of +400 vdc with a ripple of less than 7 mV and a beam current of 50^uma.

The waveguide network consists of a De Mornay-Bonardi model DEB-480 isolator, a Hewlett Packard model 532 frequency meter, a Hewlett Packard model X 424 A crystal detector and a Hewlett Packard model 382 calibrated attenuator.

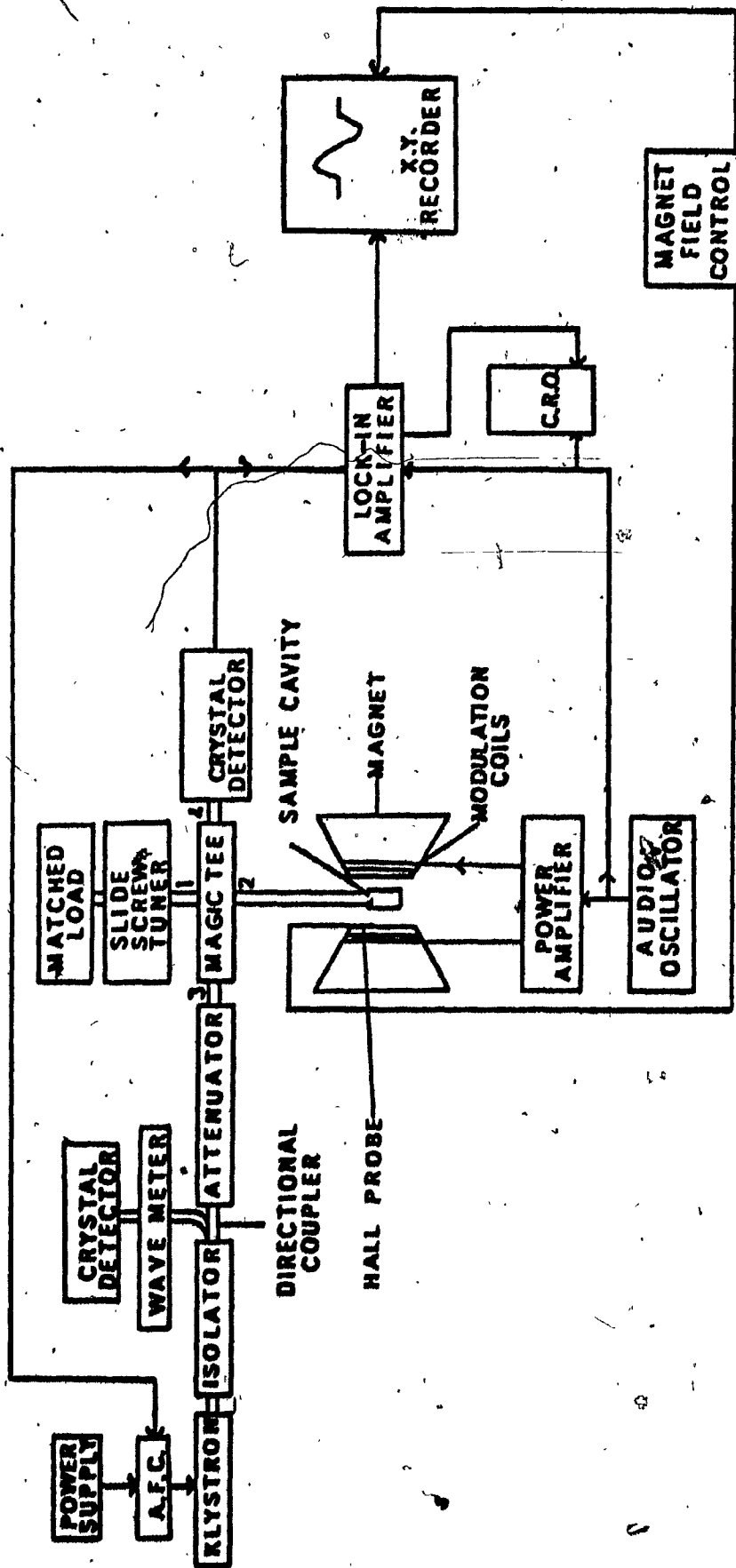


Fig. 4. Block diagram of the X-band spectrometer

The attenuator is located between the load and the generator to reduce the signal intensity incident upon the load. This is adjusted to give optimum signal to noise ratio. At room temperature due to fast relaxation times, the saturation of spin transitions is no problem, thus little or no attenuation is needed to observe a signal. However at lower temperatures, lesser power should be used to observe the resonance absorption since saturation occurs easily due to long relaxation times.

The required power from the attenuator enters arm 3 of the De Mornay-Bonardi model DB-650 magic tee where the power splits between arms 1 and 2. Arm 2 is the cavity arm which will be described later. Arm 1 is made up of a Hewlett Packard model 870 A slide screw tuner and a Hewlett Packard model 914 B matched load. The slide screw tuner is used to produce an under-coupled cavity match because the crystal detector operates more efficiently with a finite amount of power incident upon it at all times. The longitudinal position is varied until one obtains maximum leakage on the crystal detector, fig. 5, and its insertion is adjusted for about ten percent of the power incident upon the cavity.

Arm 4 is the detector arm to which is connected a Hewlett Packard model 485 B detector mount containing a 1 N23D silicon diode which provides a good signal to noise ratio.

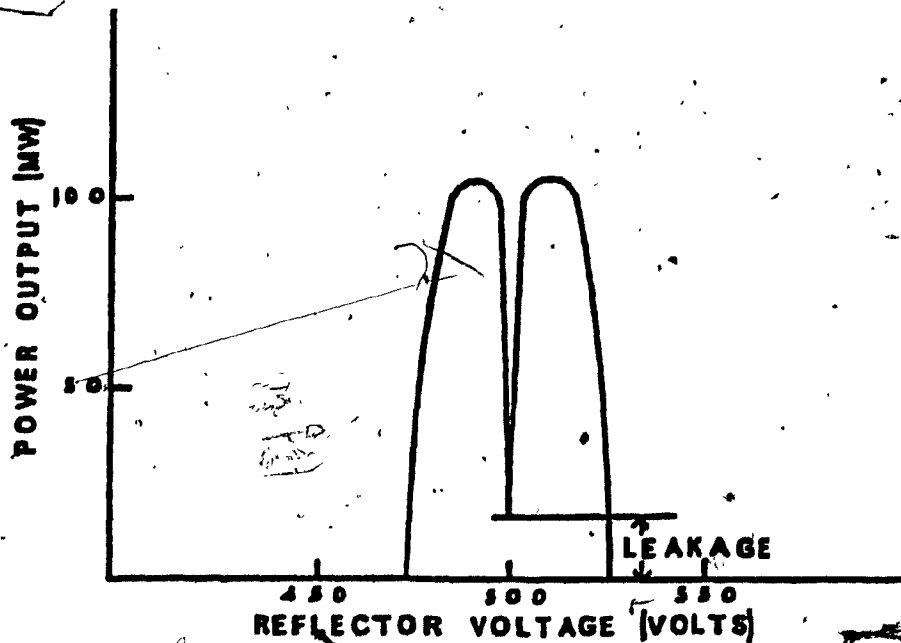


Fig. 5 Klystron mode with cavity frequency
centered on mode

Figure 6 shows a detailed view of the cavity arm of the spectrometer. This arm has been designed for use inside the cryostat thus the top flange is sealed off for evacuation purposes by means of a mica sheet and silicone cement on the outside. The cavity arm is evacuated so as to reduce condensation and thus preserve tuning of the cavity at low temperatures.

The cavity, which is gold plated, is a rectangular type, resonating in the TE_{102} mode at a frequency of about 9.46 GHz to wavemeter accuracy. The cavity is coupled to the waveguide by a 0.010 inch

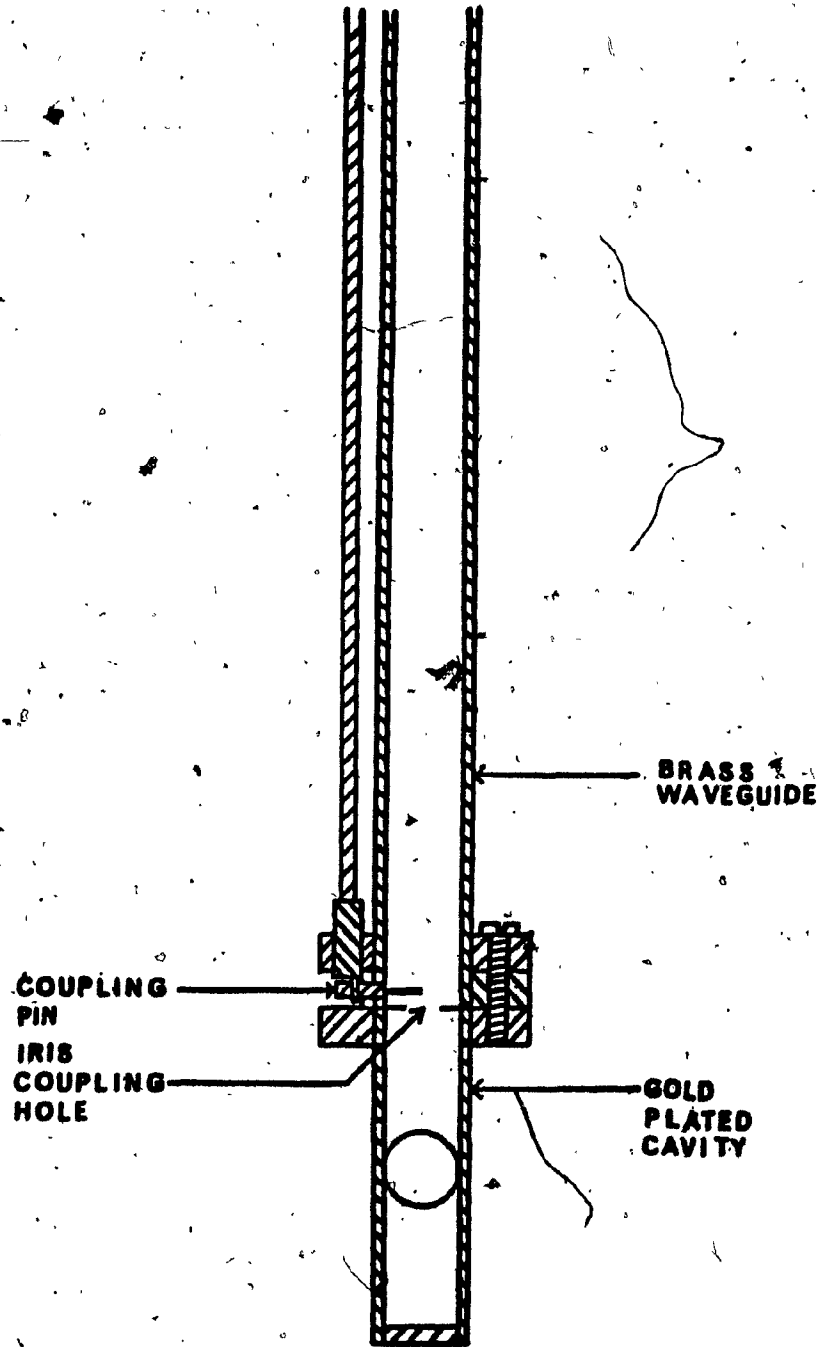


Fig. 6. Detailed view of cavity arm

gold plated brass sheet with an iris in the center of 0,20 inch diameter. The cavity is matched to the waveguide by a 0,030 inch inductive pin. The pin is connected to a cam and rod which leads to the upper flange of the cryostat. The arrangement was necessitated by the fact that the resonant frequency and the coupling of the cavity are temperature sensitive and one must be able to adjust externally at low temperatures.

The crystal detector demodulates the microwave power which is then transferred by a coaxial cable to the Princeton Applied Research model 122 lock-in-amplifier.

The magnetic field H is produced by a Varian V-3900 electromagnet which is capable of producing a field of 13 kG across a 3 inch magnet gap. Sweep ranges from 0,25 to 10 kG with sweep times of 0,50 min to 100 min can be selected.

The liquid helium cryostat shown in fig. 7 was used to obtain the spectra at liquid nitrogen and liquid helium temperatures. The totally metallic construction ¹⁹ is similar to many commercially available models. The changes allow for simultaneous electron spin resonance and Mossbauer effect experiments.

The inner tail (L) or sample region provides the environment in which the experiment is performed. Helium flows from the helium reservoir (H) via a capillary tube (N) to the bottom of the tail and then is diffused by packed fibre-glass. The rate of flow of helium is controlled by the throttle valve (O). Brass flanges with half inch

- A WAVEGUIDE
- B ELECTRICAL CONNECTOR
- C HELIUM VENT
- D HELIUM PUMPING ARM
- E NITROGEN VENT
- F OUTER SHELL
- G NITROGEN RESERVOIR
- H HELIUM RESERVOIR
- I INSULATION SPACE
- J OUTER TAIL
- K RADIATION SHIELD
- L INNER TAIL
- M BERYLLIUM WINDOWS
- N CAPILLARY TUBE
- O THROTTLE VALVE
- P THROTTLE VALVE STEM
- Q NITROGEN FILL
- R THROTTLE CONTROL

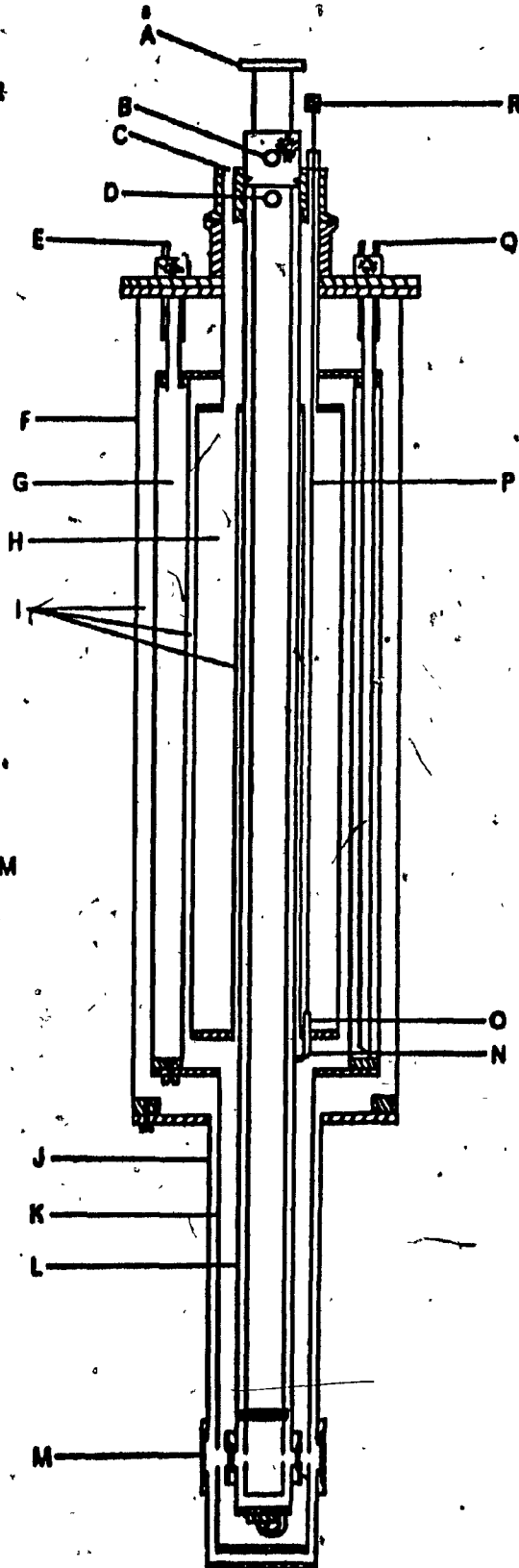


Fig. 7. The liquid helium cryostat

holes were brazed to the tail to hold 0,020 inch thick beryllium windows which were sealed by indium O-rings.

The outer tail (J) is again equipped with brass flanges and beryllium windows epoxied to them. This outer tail is hermetically sealed to the outer shell (F) by rubber O-rings.

The cryostat has two vacuum systems: an oil diffusion pump to evacuate the insulation space (I) to a pressure of no greater than 10^{-4} mm of mercury and a high speed rotary pump to reduce the vapour pressure of the helium gas to obtain temperatures below 4,2 K.

The temperature controller is an Artronix model 5301, capable of control over a range of 1,0 K to 320 K. The temperature set control is a ten turn dial which provides continuous temperature settings throughout each of the twelve ranges for sensors.

The germanium resistor had been previously calibrated from 1,61 K to 37,11 K and the platinum resistor from 29,96 K to 102,40 K. The errors with respect to the calibration curve are 0,95 percent for the germanium resistor and 0,75 percent for the platinum resistor. For temperatures higher than 102,40 K the error can be as large as 3,0 percent.

3.3 Production of the Spectra

We present here the main steps of a typical experiment.

The crystal to be investigated is mounted in the center of the cavity, on the broad side of the cavity so that H can be rotated in the ZX plane; then the cavity arm is placed in the cryostat.

The insulation space is then pumped down to a pressure of no greater than 10^{-4} mm. The sample region and the helium reservoir are purged with helium gas to prevent air from freezing in the capillary tube and in the sample region of the cryostat. The nitrogen reservoir is then filled resulting in a further decrease of pressure in the evacuation space and precooling of the overall system.

The klyatron power supply is switched on and the klyatron frequency is tuned to the resonance frequency of the cavity with the reflector voltage modulated by a 60 Hz sinusoidal signal. The magnet, modulation field, automatic frequency control and lock-in-amplifier are switched on and allowed one half hour to warm up.

After the cryostat has been allowed to cool for four to five hours the helium is transferred from a 25 litre capacity storage container via a transfer tube to the helium reservoir by applying a small pressure to the container. Once the helium remains as a liquid in the reservoir the insulation vacuum decreases rapidly to better than 10^{-9} mm of mercury. Once cryopumping begins the cryostat

is closed off, from the oil diffusion pump.

After the transfer is complete, the rotary vacuum pump is turned on to slightly reduce the pressure in the sample region and the throttle valve is opened. The temperature control is first used to monitor the cooling. At the desired temperature the heater is turned on and the temperature controlled manually. When the temperature appears to be reasonably stable the controller is turned to the automatic mode. It is important here that the stability is within .01 K as small changes in the temperature cause the cavity tuning and frequency to change.

The cavity is now tuned to the correct frequency and crystal leakage. The 60 Hz modulation is removed and the automatic frequency control is connected into the circuit.

The magnetic field is then slowly increased until a resonance absorption is found. The magnetic field is then set on a maximum of the derivative of the absorption curve plotted on the X-Y recorder. The frequency and phase of the signal channel of the lock-in-amplifier are tuned to 390 Hz, the frequency of the signal being reflected from the cavity. The time constant is adjusted for best signal to noise ratio and final adjustments are made to the microwave bridge to obtain the best representation of the absorption signal.

The magnetic field is then swept over the range of interest and the derivative of the absorption curve plotted on the X-Y recorder.

This plot constitutes the representation of the EPR spectrum.

3.4 Measurement of the Resonant Field Values

The resonant field values were obtained by means of a nuclear magnetic resonance probe containing protons, and suitable for fields of 1 kG to 8 kG.

Nuclear magnetic resonance is a well known principle and commonly used to measure magnetic fields. The resonance condition is

$$2\pi\nu = \gamma H$$

where ν is the applied frequency, γ is the magnetogyric ratio of the nucleus contained in the probe and H is the applied field. For protons this becomes

$$H = 0,23487 \nu,$$

where H is given in gauss and ν in Hz.

The instrument used to make these measurements was a Varian F-8 nuclear fluxmeter and a Hewlett Packard model 5245 N frequency counter.

To determine the magnetic field by this method, the frequency at resonance is measured for each transition line on the spectrum, with H parallel to the Z axis, producing a scale for H in other directions inside the ZX plane. The accuracy of this measurement is better than 1 part in 10^5 , but the definition of the transition, i.e. the middle of peak-to-peak width, was precise to only 1 part in 10^3 .

CHAPTER IV

DATA AND ANALYSIS

4.1st At Room Temperature

The crystal was first mounted in the ZX plane to study the angular variation of the spectrum.

With H // Z, at a temperature of 295 K, only 3 lines of each set of six possible lines are clearly identifiable, fig. 8. The remaining 6 lines had to be extrapolated from the angular variation of the spectrum, fig. 9. Figure 10 shows the spectrum obtained for Z // X.

A set of lines is clearly twice as intense as the other, (we call it set I in accordance with Daniels and Wassmeyer³) confirming that one set is due to equivalent sites twice as numerous as a third non equivalent site.

The DPPH line appears at 3350 gauss indicating a frequency of 9,347 GHz for the microwave radiation.

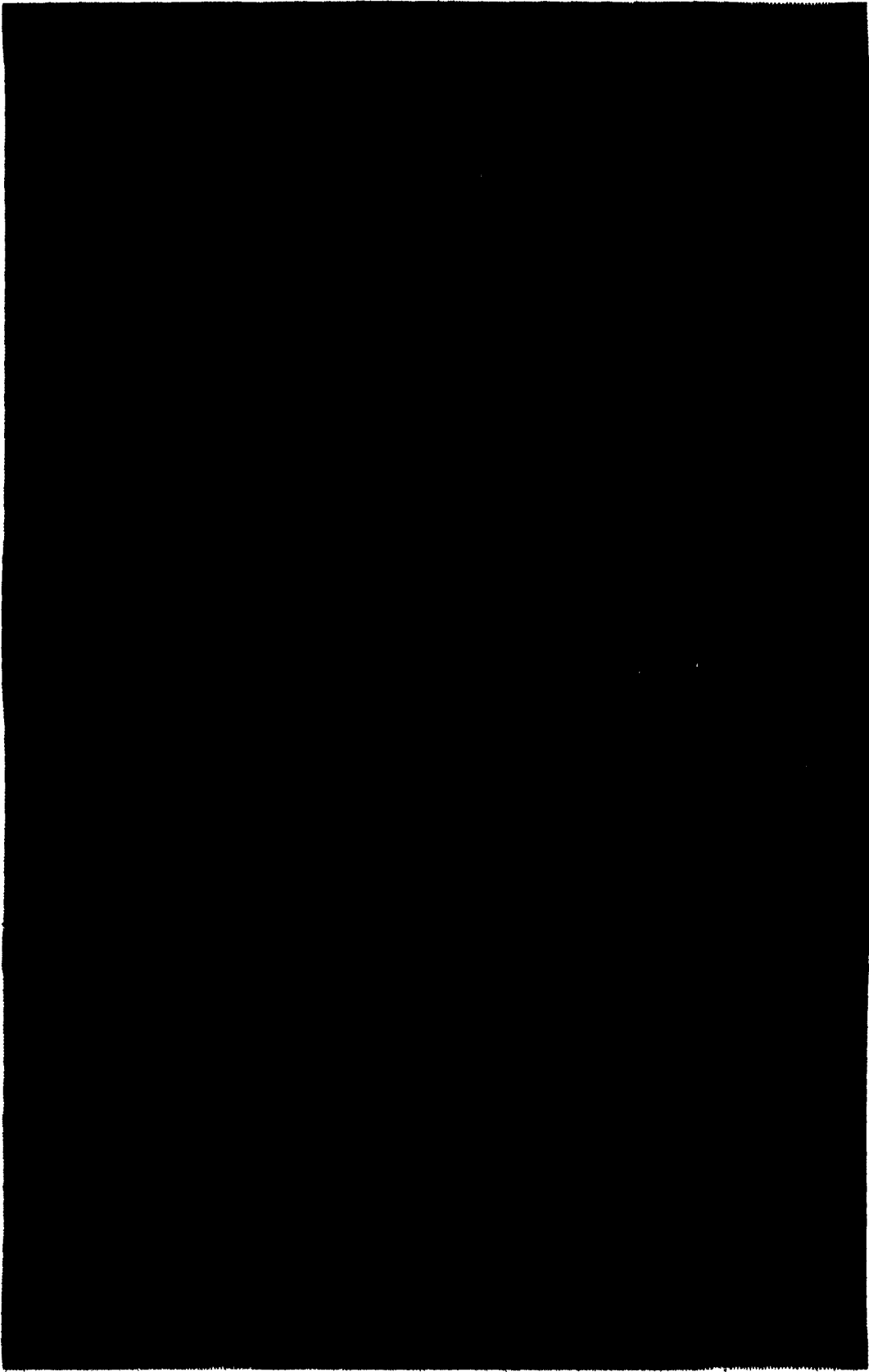


Fig. 8. Derivative of absorption curve of Cr^{3+} in GASH, at room temperature, with $H // Z$.

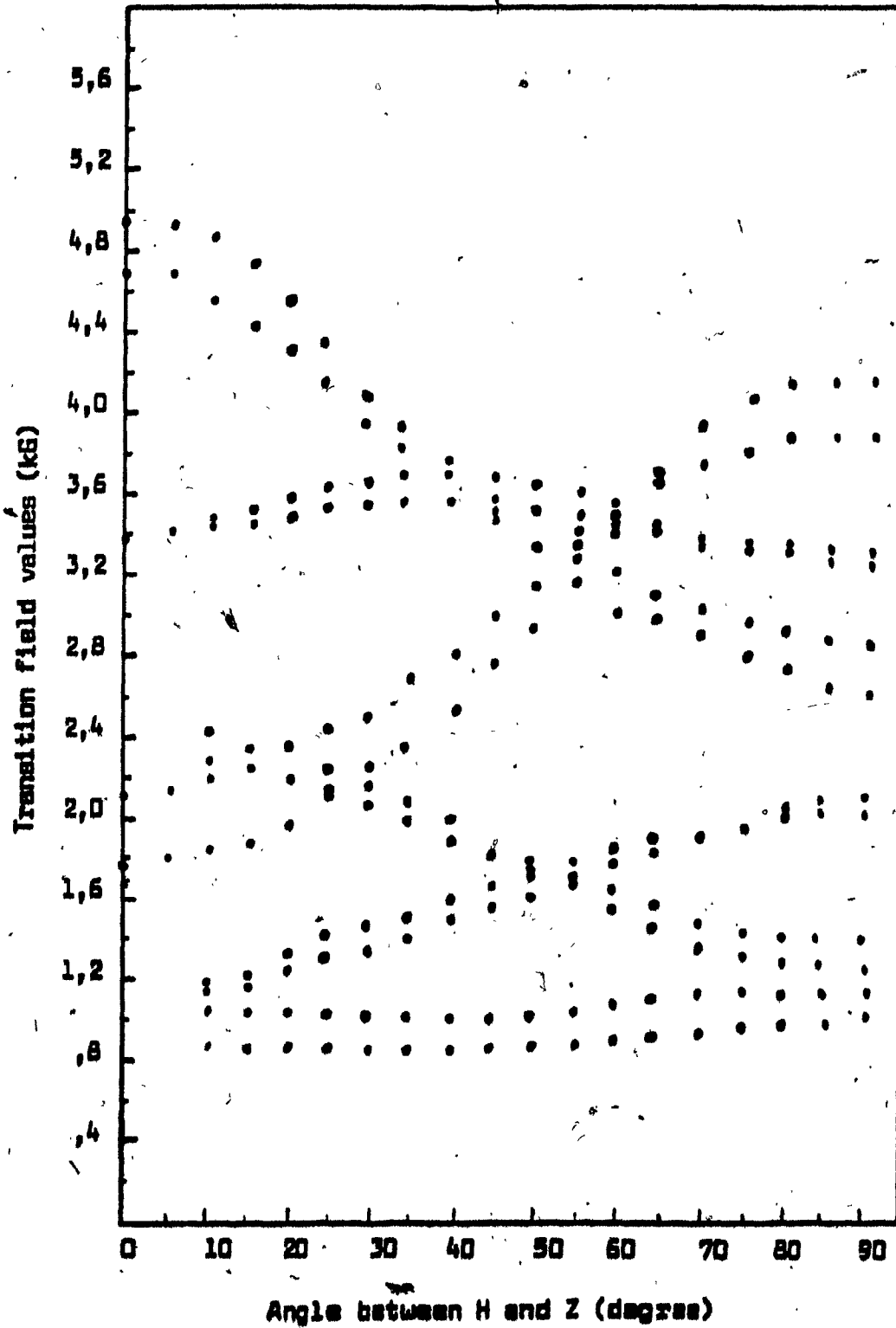


Fig. 9. Angular variation of H in the ZX plane, at room temperature

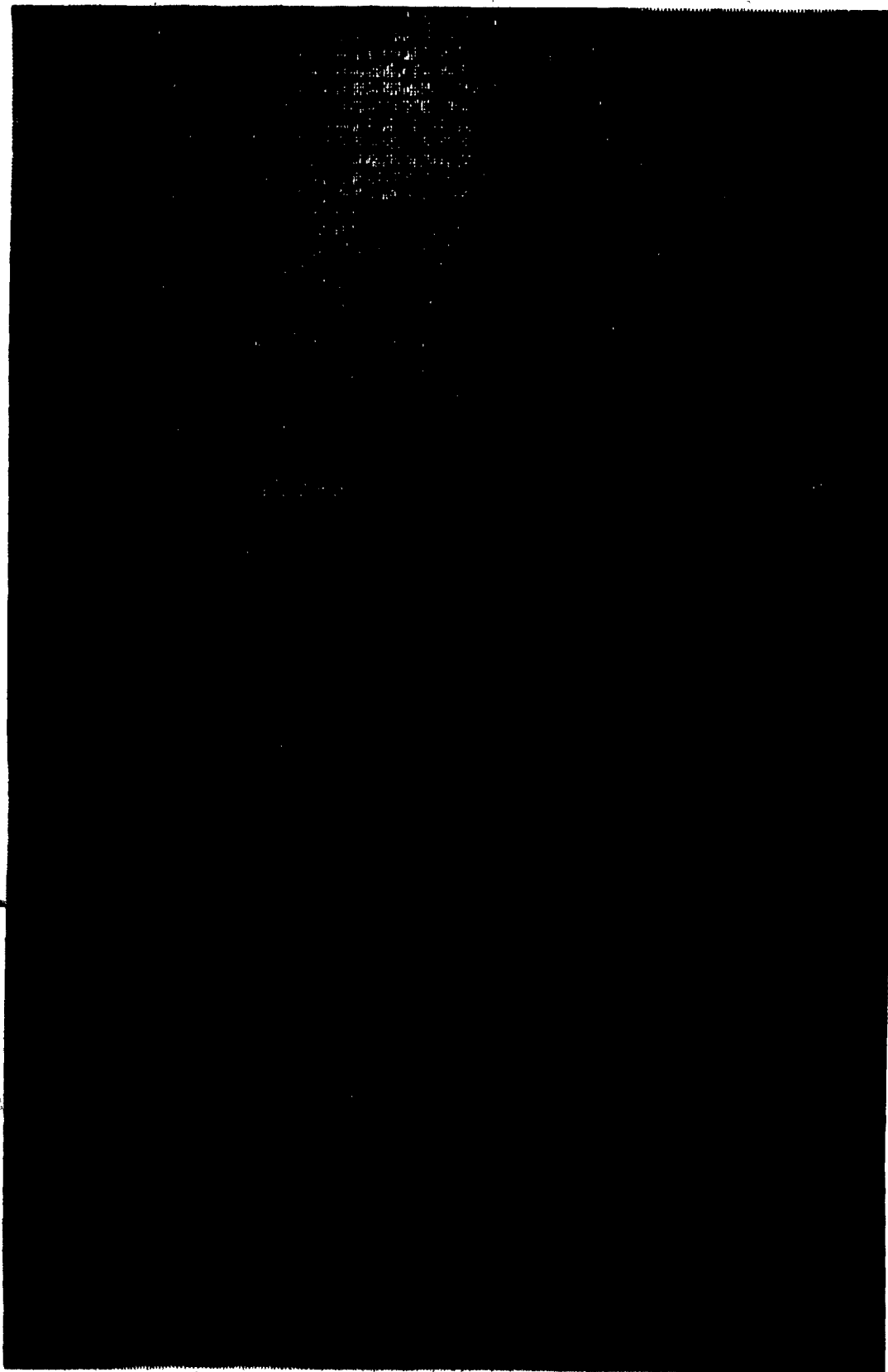


Fig. 10 Derivative of absorption curve of Cr³⁺ in GASH, at room temperature, with H // X.

Tables II a, b present all the pertinent data for H // Z and H // X, for set I and set II respectively.

Table II, a

Data from set I, at room temperature

Transition	Along Z axis			Along X axis
	Field (gauss)	Line width (gauss)	Relative amplitude	Field (gauss)
1/2 ↔ -1/2	3394	18	10,	3298
-3/2 ↔ -1/2	2127	13	3,5	4019
1/2 ↔ 3/2	4663	13	3,1	2775
-3/2 ↔ 1/2	1062	--	----	1062
-1/2 ↔ 3/2	2330	--	----	1304
3/2 ↔ -3/2	1131	--	----	1958

Table II, b

Data from set II at room temperature

Transition	Along Z axis			Along X axis
	Field (gauss)	Line width (gauss)	Relative amplitude	Field (gauss)
1/2 ↔ -1/2	3394	13	10	3240
-3/2 ↔ -1/2	1808	13	5,4	4182
1/2 ↔ 3/2	4978	13	4,8	2614
-3/2 ↔ 1/2	906	--	----	1051
-1/2 ↔ 3/2	2498	--	----	1180
3/2 ↔ -3/2	1131	--	----	1933

For each site, we used the six $|\Delta M| = 1$ lines, three for H along Z, and three for H along X, and simultaneously fitted them to produce the values of the parameters. The values obtained are given in tables III a,b, along with the values determined by Daniels and Wesemeyer³.

Table III, a

Values of parameters for set I, at room temperature

	Ours	Daniels and Wesemeyer
g_{zz}	$1,976 \pm ,003$	$1,975 \pm ,005$
g_{xx}	$1,976 \pm ,003$	$1,975 \pm ,005$
D (GHz)	$-1,754 \pm ,008$	$1,727 \pm ,015$
SMD (GHz ²)	,0009	-----

Table III, b

Values of parameters for set II, at room temperature

	Ours	Daniels and Wesemeyer
g_{zz}	$1,980 \pm ,003$	$1,975 \pm ,005$
g_{xx}	$1,980 \pm ,003$	$1,975 \pm ,005$
D (GHz)	$-2,196 \pm ,008$	$2,188 \pm ,015$
SMD (GHz ²)	,0018	-----

Our values agree very well in magnitude with those of Daniels and Wesemeyer; moreover the correctness of the fit is indicated by the small SMD values. The negative sign for D has already been

used although the evidence for it will come only at liquid helium temperature. The errors indicated are estimated maximal experimental errors; they are the same for all temperatures and sites.

We also did an angular variation of H in the XY-plane which showed that there was no variation in the position of the lines as the external magnetic field was rotated; this indicates that $g_{xx} = g_{yy}$; with tables III a,b showing that $g_{zz} = g_{xx}$, we can thus conclude that

$$g_{xx} = g_{yy} = g_{zz}$$

within experimental errors, and that the g tensor has the same value for the two sites.

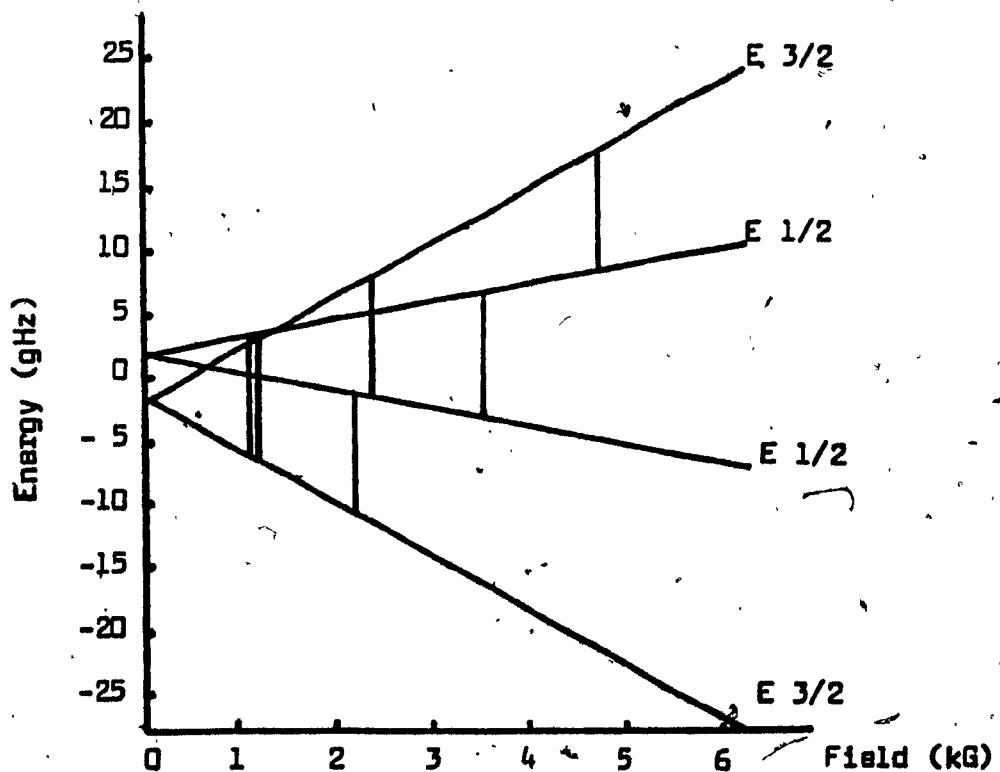


Fig. 11. Energy levels due to site I, at room temperature, with the magnetic field along Z.

Figure 11 shows the variations of the energy levels in the case of site I, at room temperature, as functions of the static magnetic field directed along the Z axis; similar diagrams could be constructed for other sites and temperatures.

4.2 At Liquid Nitrogen Temperature

At this temperature the crystal was studied only in the ZX plane.

With $H // Z$, at a temperature of 78,4 K, again only 3 lines of each set are clearly identifiable, fig. 12. The angular variation, fig. 13, discloses the positions of the other lines and allows an extrapolation of their positions for $H // Z$. Figure 14 shows the spectrum obtained for $H // X$.

The superposition of two sets of lines is again evident.

The DPPH line appears at 3355 gauss indicating a frequency of 9,409 GHz for the microwave radiation.

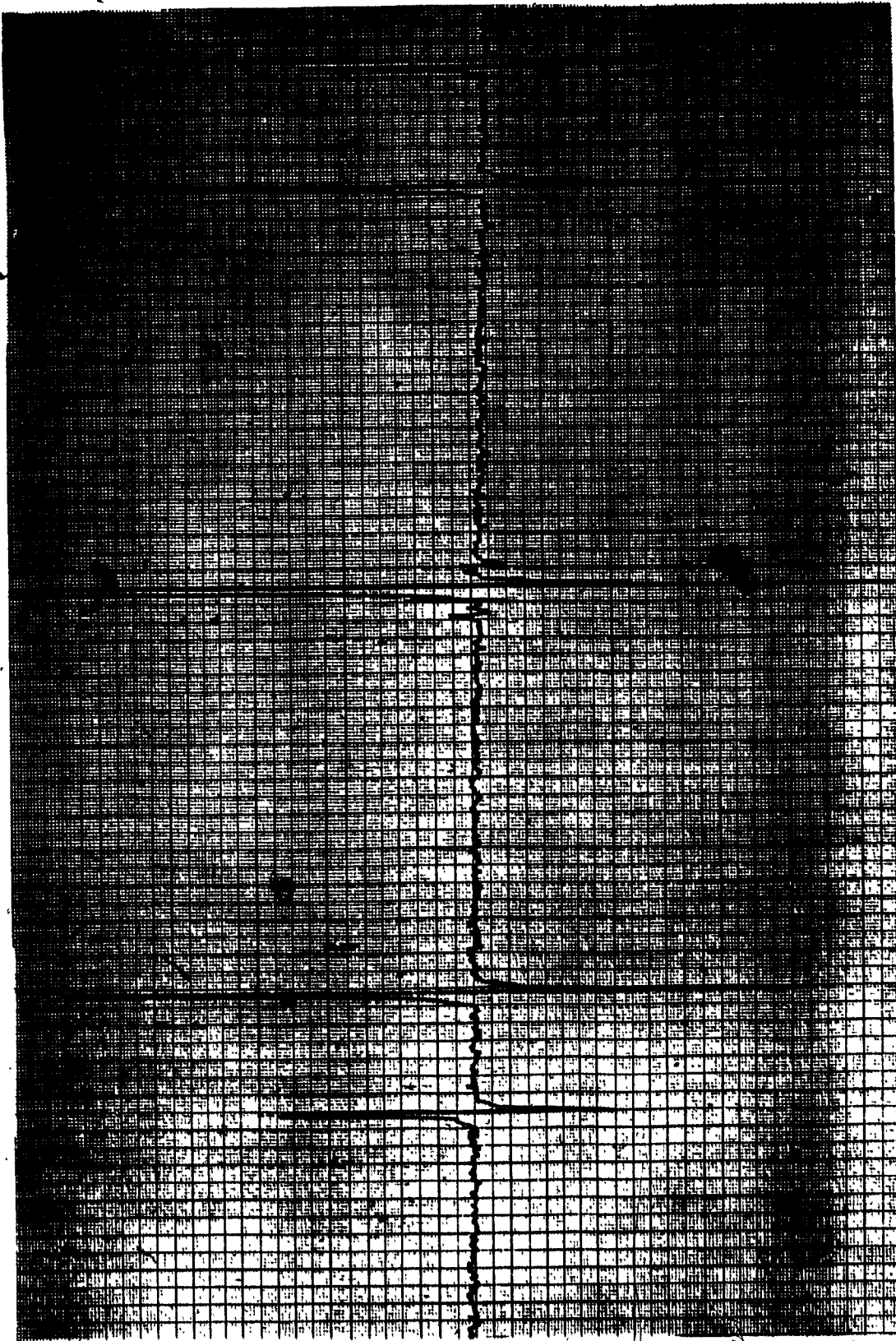


Fig. 12. Derivative of absorption curve of Cr^{3+} in GASH, at liquid nitrogen temperature, with $H // Z$.

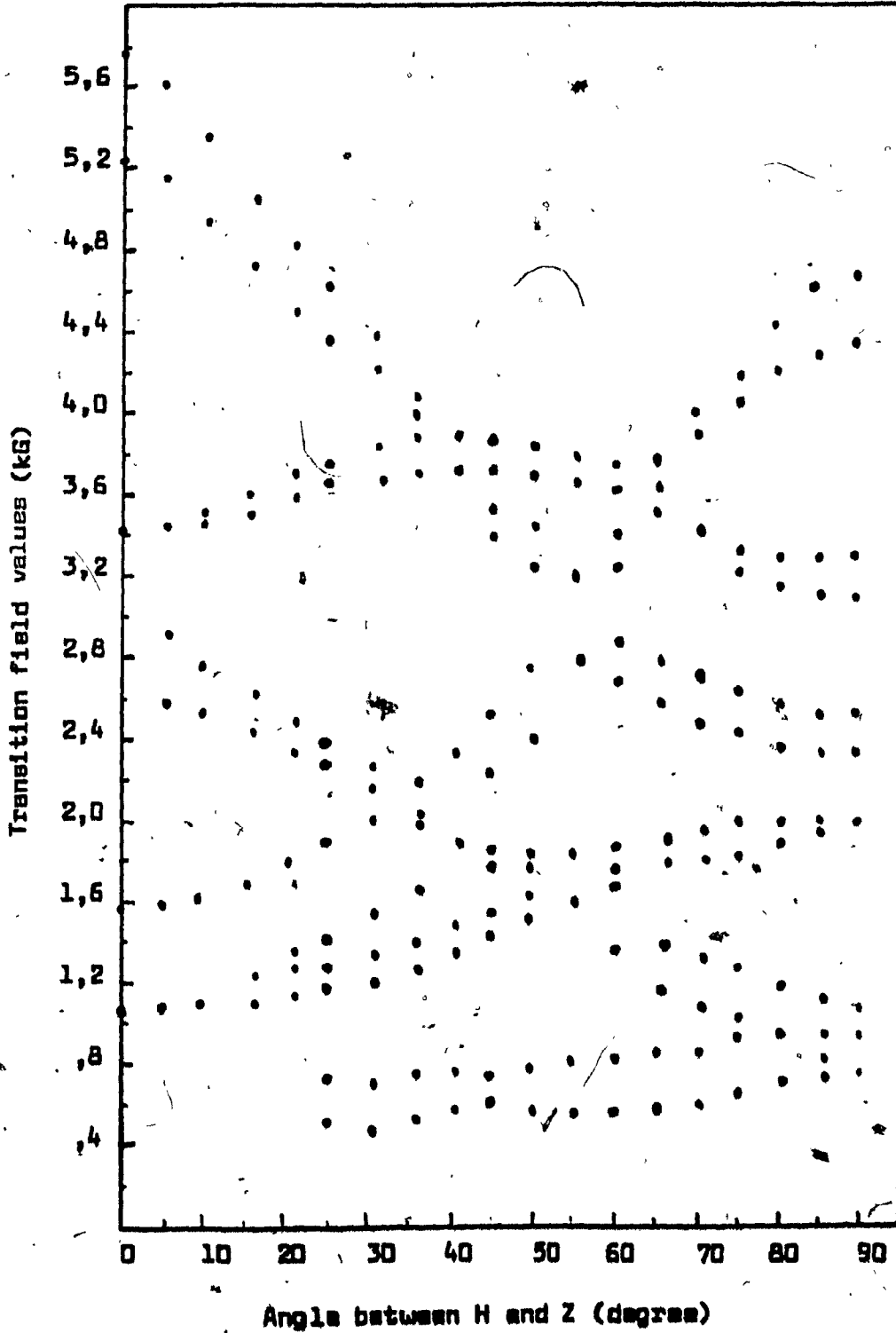


Fig. 13. Angular variation of H in the ZX plane,
at liquid nitrogen temperature



Fig. 14. Derivative of absorption curve of Cr^{3+} in GASH, at liquid nitrogen temperature, with $H // X$.

Tables IV a, b present the pertinent data for H // Z and H // X, for set I and set II respectively.

Table IV, a

Data from set I, at Liquid Nitrogen Temperature

Transition	Along Z axis			Along X axis
	Field (gauss)	Line width (gauss)	Relative amplitude	Field (gauss)
1/2 ↔ -1/2	3404	11	10	3208
-3/2 ↔ -1/2	1585	8	7,7	4297
1/2 ↔ 3/2	5218	8	7,6	2535
-3/2 ↔ 1/2	781	--	---	943
-1/2 ↔ 3/2	2610	--	---	1054
3/2 ↔ -3/2	1151	--	---	1954

Table IV, b

Data from set II, at Liquid Nitrogen Temperature

Transition	Along Z axis			Along X axis
	Field (gauss)	Line width (gauss)	Relative amplitude	Field (gauss)
1/2 ↔ -1/2	3404	11	10	3059
-3/2 ↔ -1/2	1043	8	3,9	4553
1/2 ↔ 3/2	5218	8	7,6	2535
-3/2 ↔ 1/2	781	--	---	943
-1/2 ↔ 3/2	2610	--	---	1054
3/2 ↔ -3/2	1151	--	---	1954

For each site, we used the six $|\Delta M| = 1$ lines, three for H along Z, and three for H along X, and simultaneously fitted them to produce the values of the parameters. The values obtained are given in TABLE V.

Table V

Values of the Parameters, at Liquid Nitrogen Temperature

	SET I	SET II
B_{zz}	1,976	1,976
B_{xx}	1,976	1,975
D (GHz)	-2,512	-3,261
BMD (GHz) ²	,0001	,0002

The experimental errors being the same at all temperatures, we again conclude at the isotropy of the g tensor.

4.3 At Liquid Helium Temperature

Again at this temperature, the crystal was studied only in the ZX plane.

With $H // Z$, at a temperature of 1.61 K, at least 10 of the 12 possible lines are clearly identifiable, fig. 15. The positions of only two lines have to be extrapolated from the angular variation of H in the ZX plane, fig. 16. The spectrum obtained with $H // X$ is shown on fig. 17.

A first set of lines twice as intense as the other is again evident.

The DPPH line appears at 3293 gauss, revealing that the frequency of the microwave radiation is 9,235 GHz. The reason why we had three different microwave frequencies at the three different temperatures is because the experiments at these respective temperatures were performed on a period of months and we preferred not to try to reproduce a given microwave frequency. Moreover, the resonant frequency changes as the temperature is lowered, since the dimensions of the cavity are functions of the temperature.

Tables VI a, b present the data taken from the spectra with $H // Z$ and $H // X$, for set I and set II respectively.

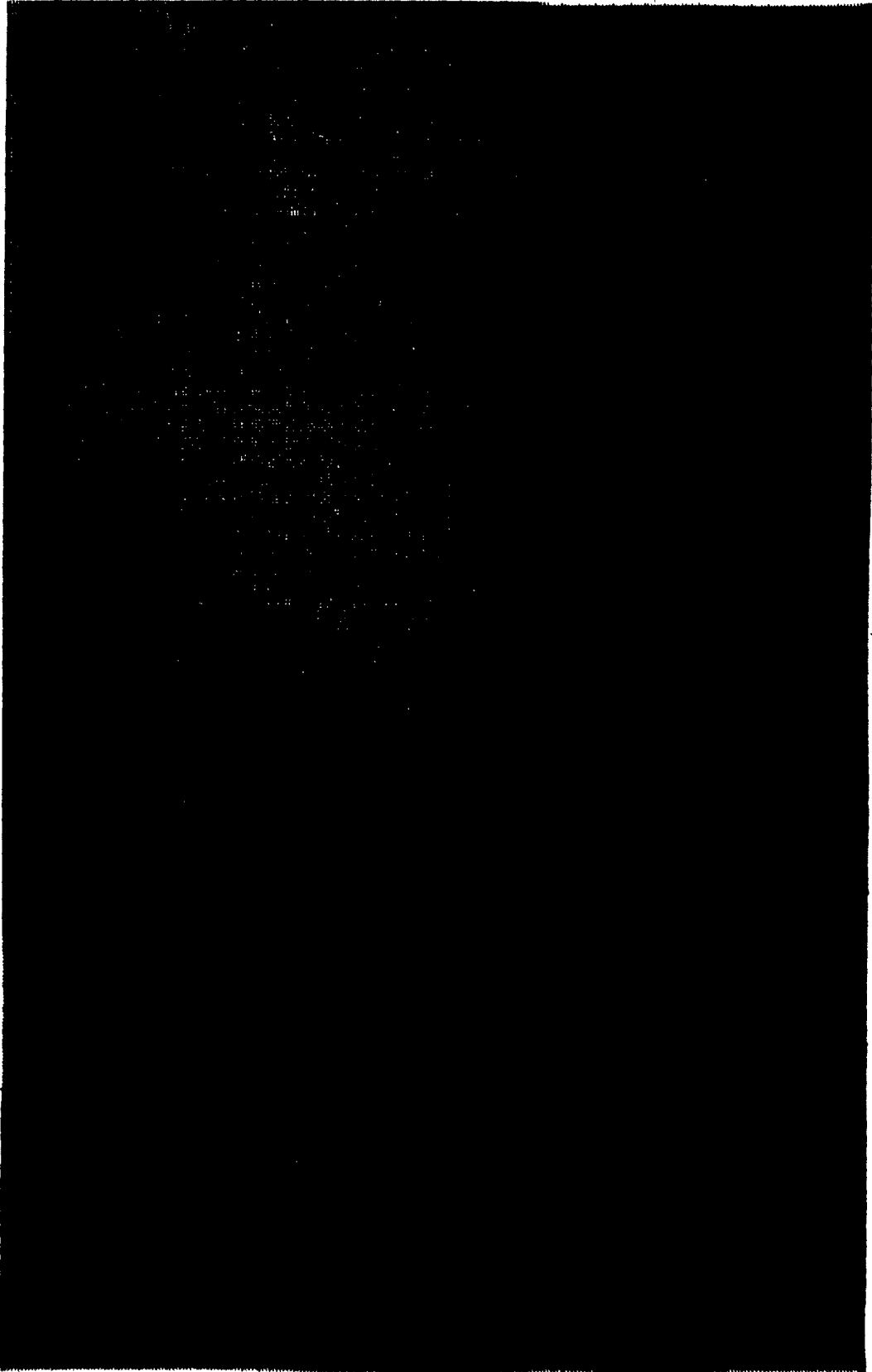


Fig. 15 Derivative of absorption curve of Cr^{3+} in EASH, at liquid helium temperature, with H // Z.

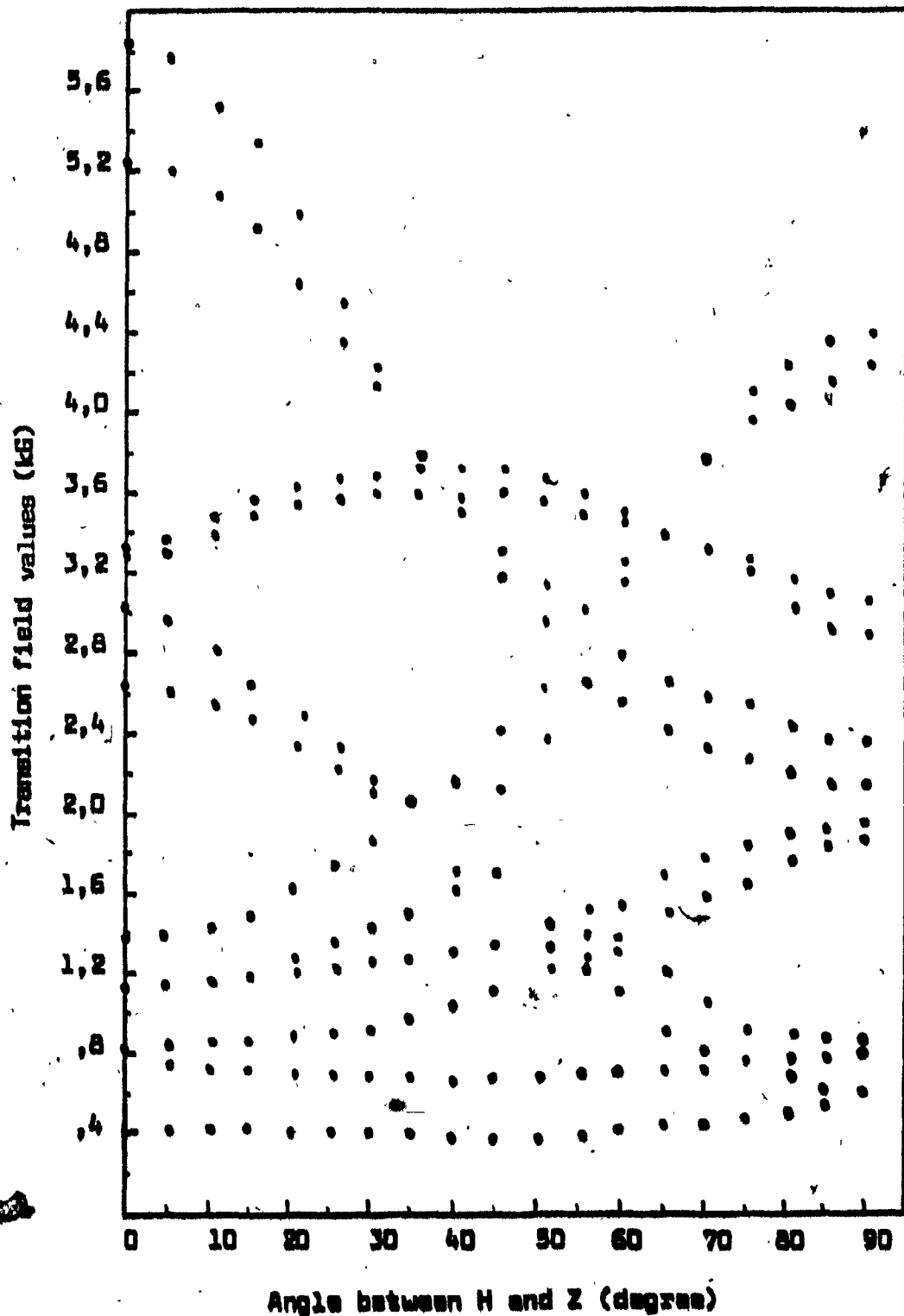


Fig. 16. Angular variation of H in the ZX plane,
at liquid helium temperature

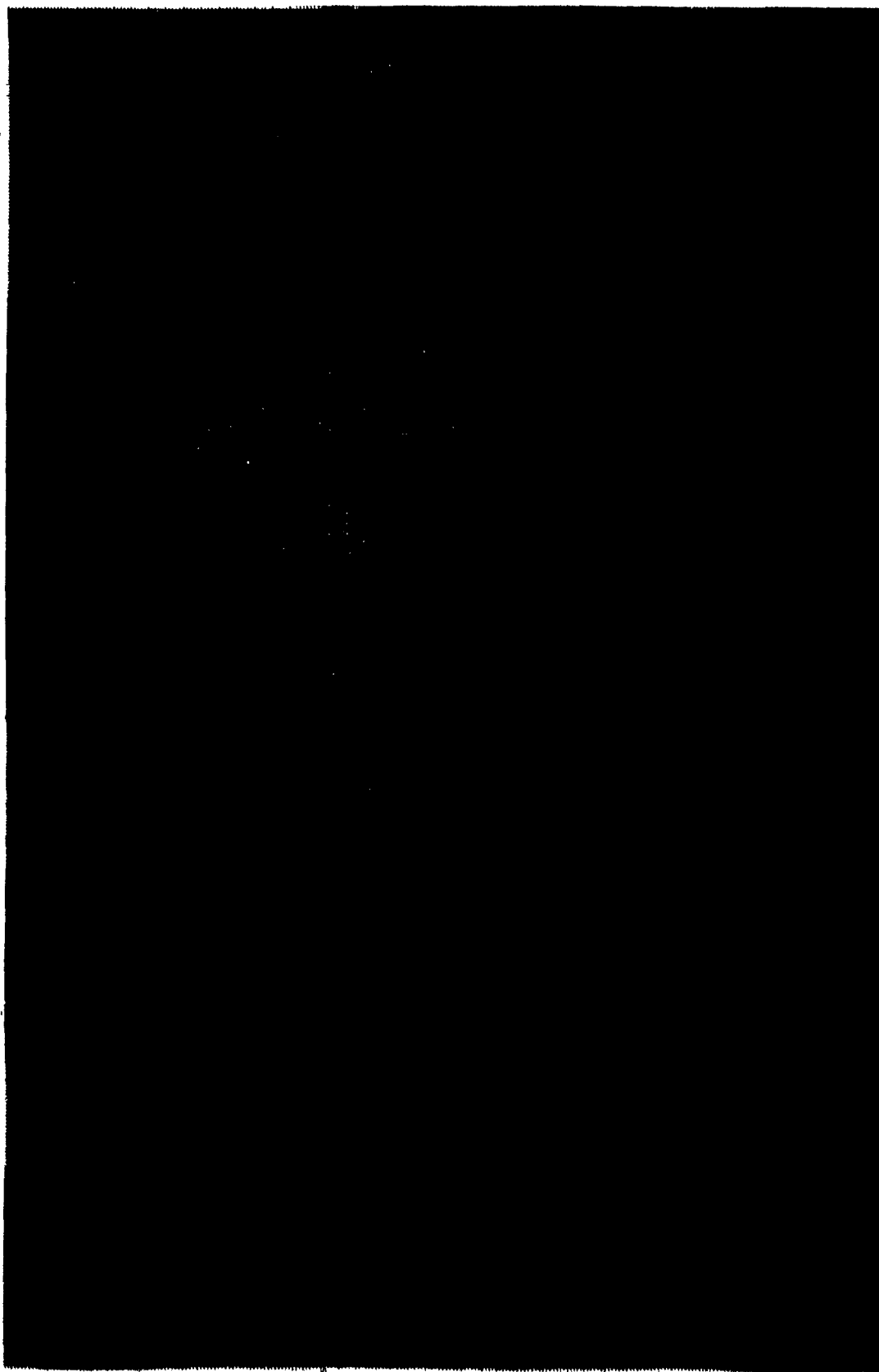


Fig. 17 Derivative of absorption curve of Cr^{3+} in EASH, at liquid helium temperature, with H // X.

Table VI, a

Data from Set I, at Liquid Helium Temperature

Transition	Along Z axis			Along X axis
	Field (gauss)	Line width (gauss)	Relative amplitude	Field (gauss)
$1/2 \leftrightarrow -3/2$	3324	18	10,	3101
$-3/2 \leftrightarrow -1/2$	1391	18	3,4	4271
$1/2 \leftrightarrow 3/2$	5238	54	2,7	2414
$-3/2 \leftrightarrow 1/2$	720	54	2,4	846
$-1/2 \leftrightarrow 3/2$	2620	18	3,7	879
$3/2 \leftrightarrow -3/2$	1107	20	1,9	1918

Table VI, b

Data from Set II, at Liquid Helium Temperature

Transition	Along Z axis			Along X axis
	Field (gauss)	Line width (gauss)	Relative amplitude	Field (gauss)
$1/2 \leftrightarrow -1/2$	3324	18	10,	2911
$-3/2 \leftrightarrow -1/2$	810	20	5,	4536
$1/2 \leftrightarrow 3/2$	5841	54	2,9	2205
$-3/2 \leftrightarrow 1/2$	423	18	5,5	603
$-1/2 \leftrightarrow 3/2$	2903	24	2,4	603
$3/2 \leftrightarrow -3/2$	1107	20	1,9	1918

As shown by the derivatives of the absorption curves, as we go from room temperature to liquid helium temperature, the intensities of the high field lines decrease, whereas those of the low field lines increase (relative to the high field ones), indicating a negative sign for D.

Fitting the transition field values and the parameters to the Hamiltonian produces the values given in table VII.

Table VII
Values of the Parameters, at Liquid Helium Temperature

	SET I	SET II
g_{zz}	1,987	1,984
g_{xx}	1,986	1,985
D (GHz)	-2,677	-3,492
SMD (GHz ²)	,0010	,0009

At liquid helium temperature we can also note the isotropy of the g tensor and its increased value with respect to the ones obtained at room temperature and liquid nitrogen temperature.

Finally the increasing trend in the magnitude of D as the temperature is lowered that was first detailed by Daniele and Wesemeyer³ is maintained down to 1,61 K.

CHAPTER V

CONCLUSION

An X-band EPR study of Cr^{3+} in GASH at room temperature, liquid nitrogen and liquid helium temperature has been presented. The values of g_{zz} , g_{xx} , D and SMD have been obtained at 295 K, 78,4 K and 1,61 K, for each of the two sites.

A negative sign for the D parameter has been deduced and its increase in magnitude with decreasing temperature has been verified down to 1,61 K.

The isotropy of the g -tensor at the three temperatures has been found, with an increase in magnitude at liquid helium temperature.


```

DIMENSION Z(20),FM(20),FC(20),DF(20),ERR(6),B(3),B1(3),B2(3,3),
1 DC(500),ABC(2),Y(4)
DIMENSION ZZ(6,6),HHOPPH(6)
DIMENSION G(J,6),GG(3,6)
DIMENSION SMD(25)
COMMON/DATA1/ABC,Y
COMMON/DATA2/DC
EQUIVALENCE (Z,DC), (FM,DC(21)), (FC,DC(41)), (DF,DC(61)), (ERR,DC(81))
1, (B,DC(101)), (B1,DC(124)), (B2,DC(137)), (N,DC(281)), (L4,DC(282)),
2 (Q1,DC(283)), (Q2,DC(284)), (M,DC(285)), (IG,DC(286)), (L,DC(287)),
3 (BO,DC(450)), (HN,DC(451)), (J2,DC(452))
EQUIVALENCE (SMD,DC(460)), (SSMD,DC(455))

```

```

DATA(G(J,1),J = 1,3)/1.976,1.976,-.5848/
DATA(G(J,2),J = 1,3)/1.976,1.976,-.7317/
DATA(G(J,3),J = 1,3)/1.975,1.975,-.8372/
DATA(G(J,4),J = 1,3)/1.975,1.975,-1.080/
DATA(G(J,5),J = 1,3)/1.986,1.986,-.8922/
DATA(G(J,6),J = 1,3)/1.986,1.986,-1.166/

```

```

DATA(ZZ(J,1),J = 1,6)/.4663,.3394,.2127,.2775,.3298,.4019/
DATA(ZZ(J,2),J = 1,6)/.4978,.3394,.1808,.2614,.3240,.4182/
DATA(ZZ(J,3),J = 1,6)/.5218,.3404,.1585,.2535,.3208,.4297/
DATA(ZZ(J,4),J = 1,6)/.5758,.3404,.1043,.2326,.3059,.4553/
DATA(ZZ(J,5),J = 1,6)/.5238,.3324,.1391,.2414,.3101,.4271/
DATA(ZZ(J,6),J = 1,6)/.5841,.3324,.0810,.2205,.2911,.4536/

```

```

DATA(HHOPPH(J),J = 1,6)/.3350,.3350,.3355,.3355,.3293,.3293/

```

```

DATA(ABC=2HNO,3HYES), (Y=1H,1HC,1H*,1HM)

```

```

188 FORMAT(1H1)

```

```

8 FORMAT(1X,4HQ1 = ,E13.5,5X,4HQ2 = ,E13.5)

```

```

137 FORMAT (3X,12,5X,E16.6/)

```

```

136 FORMAT(10X,19H INITIAL PARAMETERS//3X,1HJ,10X,4HB(J)//)

```

```

135 FORMAT(1X,11H PARAMETERS//3X,1HJ,10X,4HB(J),27X,6HERRORS//)

```

```

9 FORMAT(2X,4H HN= ,F9.4)

```

```

140 FORMAT(3X,12,5X,E16.6,15X,E16.6/)

```

```

138 FORMAT(5X,14H CASE NUMBER =,I2//)

```

```

141 FORMAT(10X,6H SMD =,E13.5//)

```

```

235 FORMAT (15X,5(E13.5,8X)//)

```

```

NCASES=6

```

```

NUMBER = 1

```

```

M = 3

```

```

J2 = 3

```

```

NO = 1

```

```

N = 6

```

```

L4 = 20

```

```

Q1 =1.E-8

```

```

Q2 =1.E-40

```

```

BO=92.732/6.625P

```

```

WRITE (6,188)

```

```

1 CONTINUE

```

```

DO 210 LL=1,3

```

```

210 B(LL)=G(LL,NUMBER)

```

```

WRITE (6,138) NUMBER

```

```

WRITE (6,136)

```

```

WRITE (6,137) (J,B(J),J=1,M)

```

```

WRITE(6,150)

```

```

WRITE(6,151) (ZZ(J,NUMBER),J = 1,N)

```

```
150 FORMAT(15X,26H VALUES OF MAGNETIC FIELD//)
151 FORMAT(25X,F6.4//)
DO 3 IJK = 1,6
3 Z(IJK) = ZZ(IJK,NUMBER)
HOPPH = HHOPPH(NUMBER)
WRITE(6,8) Q1,Q2
HN=HOPPH*80*2.0037
WRITE(6,9) HN
DO 201 IX = 1,6
ERR(IX) = 1.0
201 FM(IX) = HN
CALL CURFIT
SMD(NUMBER) = SSMD
WRITE(6,188)
WRITE(6,135)
DO 220 LL=1,3
220 GG(LL,NUMBER) = B(LL)
WRITE(6,140) (J,B(J),B1(J),J=1,M)
WRITE(6,188)
CALL PLOTB(NO,N,FC,FM)
WRITE(6,188)
NUMBER = NUMBER + 1
IF (NUMBER - NCASES) 1,1,2
2 CONTINUE
DO 230 LL=1,NCASES
WRITE(6,138) LL
WRITE(6,141) SMD(LL)
230 WRITE(6,235) (GG(LM,LL),LM=1,3)
STOP
END
```

C
C
C
C
C

SUBROUTINE CURFIT

EXAM HANDLES ALL MATRICES OF DIMENSIONS UP TO THE DIMS.MM OF A,B,C THAT IS M IS LESS THAN OR EQUAL TO MM (SAME IS TRUE OF MATINV AND JACOBI)

F O R T R A N

```

DIMENSION Z(20),FM(20),FC(20),DF(20),ERR(20),B(3),B1(3),B2(3,3),
1 DC(500),ABC(2),Y(4),X(20),GRAD(3),D1(3),D2(3,3),B3(3,3)
DIMENSION SMD(25)
COMMON/DATA1/ABC,Y
COMMON/DATA2/DC
EQUIVALENCE (Z,DC),(FM,DC(21)),(FC,DC(41)),(DF,DC(61)),(ERR,DC(81)
1),(B,DC(101)),(B1,DC(124)),(B2,DC(137)),(N,DC(281)),(L,DC(282)),
2(Q1,DC(283)),(Q2,DC(284)),(M,DC(285)),(IG,DC(286)),(L,DC(287)),
3(GRAD,DC(104)),(D1,DC(288)),(D2,DC(300)),(BO,DC(450)),(HN,DC(451))
4,(J2,DC(452))
EQUIVALENCE (SMD,DC(460)),(SSMD,DC(455))
DATA(ABC=2HNO,3HYES),(Y=1H,1HC,1H*,1HM)
L1 = 0
SA = 0.0
DO 1000 JG = 1,3
B1(JG) = 0.0
DO 1000 K=1,3
1000 B2(JG,K) = 0.0
L=1
DO 100 MG= 1, 6
IG = MG
X(MG)= ERR(MG)**2
CALL FUNC(2)
DF(MG)=FM(MG) - FC(MG)
DO 101 JG = 1,3
B1(JG) = B1(JG) - (2.0 * DF (MG) * D1(JG))/X(MG)
DO 101 K=1,3
101 B2(JG,K) = B2(JG,K) - (2.0 * (DF(MG) * D2(JG,K) - D1(JG) *
* D1(K)))/X(MG)
100 SA = SA + DF(MG)**2/X(MG)
GMOD=0.0
DO 102 JG = 1,3
102 GMOD=GMOD+B1(JG)**2
WRITE(6,243)SA,GMOD
243 FORMAT (1X,26H*INITIAL VALUE SUM OF SQ.=E13.5,20X,17H*SQ MOD OF GR
1AD =E13.5)
WRITE(6,1751)
1751 FORMAT(14H0 DERIVATIVES-)
WRITE(6,240)(B1(JG),JG = 1,M)
240 FORMAT (15X,5(E13.5,8X)/)
IF (SA = 0) 110, 110, 200
110 LE = 1
GO TO 600
200 S = 0.0
GMOD = 0.0
BMOD = 0.0
PROD = 0.0
AZ=ABC(1)
DO 210 JG= 1, 3
B1(JG)= 0.0

```

```
DO 210 K = 1, 3
210 B2(JG,K) = 0.0
    L = 1
    DO 220 MG = 1, 6
        IG = MG
        CALL FUNC(2)
        DF(MG) = FM(MG) - FC(MG)
        DO 220 JG = 1, 3
            B1(JG) = B1(JG) - (2.0 * DF(MG) * D1(JG))/X(MG)
        DO 220 K = 1, 3
220 B2(JG,K) = B2(JG,K) - (2.0 * (DF(MG) * D2(JG,K) - D1(JG) *
    * D1(K)))/X(MG)
    DO 230 JG = 1, 3
230 GRAD(JG) = B1(JG)
    LI = LI + 1
    CALL EXAM (B2,B1,M,LF)
    IF (LF) 250, 250, 305
250 DO 231 II = 1, 3
    DO 231 JJ = 1, 3
231 B3(II,JJ) = B2(II,JJ)
    CALL JACOBI1(M,B3,1, NR,B2)
    DO 235 MG = 1, 3
235 B1(MG) = B3(MG,MG)
    A2 = ABC(2)
    DO 260 JG = 1, 3
260 D1(JG) = 0.0
    DO 270 JG = 1, 3
    DO 270 K = 1, 3
270 D1(K) = D1(K) + B2(JG,K) * GRAD(JG)
    DO 275 JG = 1, 3
    IF (B1(JG)) 280, 290, 285
280 B1(JG) = - B1(JG)
285 D1(JG) = D1(JG)/B1(JG)
    GO TO 275
290 D1(JG) = 0.0
295 CONTINUE
    DO 295 JG = 1, 3
295 B1(JG) = 0.0
    DO 300 JG = 1, 3
    DO 300 K = 1, 3
300 B1(JG) = B1(JG) + B2(JG,K) * D1(K)
305 DO 310 JG = 1, 3
    GMOD = GMOD + GRAD(JG)**2
    BMOD = BMOD + B1(JG)**2
310 PROD = PROD + GRAD(JG) * B1(JG)
    IF (GMOD = 02) 315, 315, 320
315 LE = 2
    WRITE(6,1761) GMOD
1761 FORMAT(IX,7H GMOD =,E13.3//)
    GO TO 400
320 C = PROD/SQRT(RMOD*GMOD)
    IF (C) 335, 335, 400
335 LE = 4
    GO TO 400
400 LD = 0
    L3 = 0
```



```
DO 410 JG= 1, 3
410 GRAD(JG)= B(JG)- B1(JG)
L=2
450 DO 420 MG= 1, 6
IG = MG
CALL FUNC (1)
DF(MG)= FM(MG)- FC(MG)
420 S = S + DF(MG)**2/X(MG)
IF (SA - S) 435, 500, 500
435 LD = LD + 1
430 DO 440 JG= 1, 3
B1(JG)= B1(JG)/2.0
440 GRAD(JG)= B(JG)- B1(JG)
S = 0.0
LJ = LJ + 1
IF (LJ - 256) 450, 460, 460
460 LE = 5
GO TO 600
500 IF (LD) 505, 505, 506
506 LD = 0
GO TO 430
505 DO 510 JG= 1, 3
510 B(JG)= GRAD(JG)
SA = S
IF (SA - 01) 507, 507, 530
507 LE = 1
GO TO 600
530 IF (L4) 200, 200, 900
900 WRITE(6,920)L1,A2,L3,S,GMOD,(B(JG),JG = 1,M)
920 FORMAT(/,15H ITERATION NO.=15,10X,43H TRANSFORMATION MADE TO PR
INCIPAL AXES = A4,10X, 18H BINARY CHOP USED=13,6H TIMES/1X,27H W
EIGHTED SUM OF SQUARES = E14,7,25X,32H SQUARE MODULUS OF GRADIE
NT = E14,7/20H PARAMETERS B(JG)=/(6E17.8)/)
IF (L1 - L4) 200, 910, 910
910 LE = 6
GO TO 600
600 DO 710 JG = 1,3
B1(JG)= 0.0
DO 710 K=1,3
710 B2(JG,K)= 0.0
L=1
DO 720 MG= 1, 6
IG = MG
CALL FUNC(2)
DF(MG)= FM(MG)- FC(MG)
DO 720 JG= 1, 3
B1(JG) = B1(JG) - (2.0 * DF(MG) * D1(JG))/X(MG)
DO 720 K = 1, 3
720 B2(JG,K) = B2(JG,K) - (2.0 * (DF(MG) * D2(JG,K) - D1(JG) *
D1(K)))/X(MG)
CALL MATINV(B2,M,B1,1,DETERM)
```

```
DO 730 JG = 1,3
IF (B2(JG,JG)) 2001,2001,2002
2001 B1(JG) = -SQRT(-B2(JG,JG))
998  FORMAT (10H B1(JG) =,E16.6/)
WRITE (6,998) B1(JG)
GO TO 730
2002 B1(JG) = SQRT(B2(JG,JG))
730  CONTINUE
DO 740 JG = 1,3
DO 740 K=1,3
740  B2(JG,K) = B2(JG,K)/(B1(JG) * B1(K))
WRITE(6,551)LE,SA
551  FORMAT(//,13H EXIT NUMBER=I3,25X,25H WEIGHTED SUM OF SQUARES=E15.8
//)
SSMD = SA
RETURN
END
```

```

SUBROUTINE FUNC(LX)
C  SUBROUTINE FUNC
  DIMENSION DC(300),B(3,2),D1(3),D2(3,3),FC(20),Z(20),Q(4),S(4,
14),R(4,4),SIGN(14),SP(4,4)
  COMMON/DATA2/DC
  EQUIVALENCE (Z,DC),(FC,DC(41)),(B,DC(101)),(D1,DC(288)),(D2,DC(30
1)),(M,DC(285)),(L,DC(287)),(IG,DC(286)),(BO,DC(450)),(MN,DC(451))
  Z,(JZ,DC(452))
  DATA(SP(J,1),J=1,4)/1.5,.5,-.5,-1.5/
  DATA(SP(J,3),J=1,4)/ 3.,-3.,-3., 3./
  RE=SQRT(2.0)
  R3=SQRT(3.0)
  R5=SQRT(5.0)
  R7=SQRT(7.0)
  SP(1,4) = R3
  SP(2,4) = R3
  SP(4,1) = SP(1,4)
  SP(4,2) = SP(2,4)
  IF (Z(IG)) 18,21,18
18 CONTINUE
  IF(IG = JZ) 19,19,20
19 CONTINUE
  DO 100 IX=1,4
  DO 100 JX=1,4
  S(IX,JX) = 0.0
100 R(IX,JX) = 0.0
  PBB=B(1,L)*BO*Z(IG)
  S(1,1) = 1.5 * PBB + 3 * B(3,L)
  S(2,2) = .5 * PBB - 3 * B(3,L)
  S(3,3) = -.5 * PBB - 3 * B(3,L)
  S(4,4) =-1.5 * PBB + 3 * B(3,L)
207 CONTINUE
  CALL JACOBI(4,5,1,NR,R)
  I9=IG + 1
  FC(IG) = ABS(S(IG,IG) - S(I9,I9))
  SIGN(IG) = (S(IG,IG) - S(I9,I9))/FC(IG)
  GO TO 17
20 CONTINUE
  Q(3) = -(B(3,L))/2.
  Q(4) = -(3.* B(3,L))/2.
  DO 101 IX=1,4
  DO 101 JX=1,4
  S(IX,JX) = 0.0
  R(IX,JX) = 0.0
101 CONTINUE
  PBB =B(2,L)*BO*Z(IG)
  S(1,1) = 1.5 * PBB + 3 * Q(3)
  S(2,2) = .5 * PBB - 3 * Q(3)
  S(3,3) = -.5 * PBB - 3 * Q(3)
  S(4,4) =-1.5 * PBB + 3 * Q(3)
  S(1,3) = SQRT(3.0) * Q(4)
  S(2,4) = S(1,3)
  DO 307 IX = 1,4
  DO 307 JX = 1,4
  IF (IX =JX) 306,306,305

```

```
305 S(IX,JX) = S(JX,IX)
306 CONTINUE
307 CONTINUE
CALL JACOBI(4,S,1,NR,R)
I6 = I6 - 2
I7 = I6 - 3
FC(I6) = ABS(S(I7,I7) - S(I6,I6))
SIGN(I6) = (S(I7,I7) - S(I6,I6))/FC(I6)
GO TO 17
21 CONTINUE
FC(I6) = HN
SIGN(I6) = 1.
17 CONTINUE
IF (LX = 1) 110,110,120
120 CONTINUE
DO 235 IZ=1,3
D1(IZ) = 0.0
DO 235 IJ=1,3
235 D2(IZ,IJ) = 0.0
TEMP1 = 0.
IF (Z(I6)) 418,217,418
418 CONTINUE
DO 236 IT=1,4
IF (I6 = J2) 401,401,402
401 CONTINUE
I8 = I6 + 1
RR1 = (R(IT,I6) * R(IT,I6) - R(IT,I8) * R(IT,I8)) * SIGN(I6)
GO TO 403
402 CONTINUE
IL=I6 - 3
IL8=IL+1
RR1=(R(IT,IL)**2 - R(IT,IL8)**2)*SIGN(I6)
403 CONTINUE
D1(1) = SP(IT,1)*RR1*BO*Z(I6)+D1(1)
D1(2) = 0.
236 D1(3) = SP(IT,3)*RR1 *D1(3)
DO 237 IT=1,2
ITR = IT + 2
IF(I6 = J2)407,407,406
406 CONTINUE
IL=I6 - 3
IL8=IL+1
RR2=2.*(R(IT,IL)*R(ITR,IL) - R(IT,IL8)*R(ITR,IL8))*SIGN(I6)*R3
TEMP1 = RR2 * TEMP1
407 CONTINUE
237 CONTINUE
IF(I6 = J2) 217,217,220
220 CONTINUE
D1(2) =D1(1)
D1(1) =0.0
TEMP =D1(3)
D1(3) = - (TEMP)/2. - 1.5 * TEMP1
217 CONTINUE
110 CONTINUE
RETURN
END
```

```

SUBROUTINE EXAM(A,B,M,LF)
SUBROUTINE EXAM
  C
  C
  F O R T R A N *
  DIMENSION A(3,3),B(3),C(3)
  DO 80 J=1,M
80  C(J)=A(J,J)
  IF(A(1,1)) 60,200,70
60  A(1,1) =-SQRT(-A(1,1))
  GO TO 300
70  A(1,1) =SQRT(A(1,1))
  GO TO 100
100 IF(M=1)400,400,110
110 DO 115 K=2,M
115 A(1,K)=A(1,K)/A(1,1)
  DO 120 J=2,M
  J1=J-1
  S=A(J,J)
  DO 125 L=1,J1
125 S=S-A(L,J)*2
  IF (S) 50,200,40
50  A(J,J) =-SQRT(-S)
  GO TO 300
40  A(J,J) =SQRT(S)
  GO TO 130
130 IF(J=M)135,400,400
135 J2=J+1
  DO 120 K=J2,M
  S=A(J,K)
  DO 145 L=1,J1
145 S=S-A(L,J)*A(L,K)
120 A(J,K)=S/A(J,J)
400 B(1)=B(1)/A(1,1)
  IF(M=1)420,420,405
405 DO 410 J=2,M
  S=B(J)
  J1=J-1
  DO 415 L=1,J1
415 S=S-A(L,J)*B(L)
410 B(J)=S/A(J,J)
420 B(M)=B(M)/A(M,M)
  J=M-1
435 IF(J)450,450,425
425 S=B(J)
  J2=J+1
  DO 430 L=J2,M
430 S=S-A(J,L)*B(L)
  B(J)=S/A(J,J)
  J=J-1
  GO TO 435
450 LF=1
  GO TO 460
200 LF=0
  GO TO 460
300 LF=-1
460 DO 465 J=1,M
  A(J,J)=C(J)
  IF(J=M)470,475,475
470 J2=J+1
  DO 465 K=J2,M
465 A(J,K)=A(K,J)
475 RETURN
  END
```

```
SUBROUTINE MATINV(A,N,B,M,DETERM)
C MATRIX INVERSION WITH ACCOMPANYING SOLUTION OF LINEAR EQUATIONS
  DIMENSION IPIVOT(3),A(3,3),B(3,1),INDEX(3,2),PIVOT(3)
  EQUIVALENCE (IROW,JROW),(ICOLUMN,JCOLUMN),(AMAX,T,SWAP)
  DETERM=1.0
  DO 20 J=1,N
20  IPIVOT(J)=0
  DO 50 I=1,N
  AMAX=0.0
  DO 105 J=1,N
  IF(IPIVOT(J)-1)60,105,60
60  DO 100 K=1,N
  IF(IPIVOT(K)-1)80,100,740
80  IF(ABS(AMAX)-ABS(A(J,K)))85,100,100
85  IROW=J
  ICOLUMN=K
  AMAX=A(J,K)
100 CONTINUE
105 CONTINUE
  IPIVOT(ICOLUMN)=IPIVOT(ICOLUMN)+1
  IF (IROW-ICOLUMN)140,260,140
140 DETERM=-DETERM
  DO 200 L=1,N
  SWAP=A(IROW,L)
  A(IROW,L)=A(ICOLUMN,L)
200 A(ICOLUMN,L)=SWAP
  IF(M)260,260,210
210 DO 250 L=1,M
  SWAP=B(IROW,L)
  B(IROW,L)=B(ICOLUMN,L)
250 B(ICOLUMN,L)=SWAP
260 INDEX(I,1)=IROW
  INDEX(I,2)=ICOLUMN
  PIVOT(I)=A(ICOLUMN,ICOLUMN)
  DETERM=DETERM*PIVOT(I)
  A(ICOLUMN,ICOLUMN)=1.0
  DO 350 L=1,N
350 A(ICOLUMN,L)=A(ICOLUMN,L)/PIVOT(I)
  IF(M)380,380,360
360 DO 370 L=1,M
370 B(ICOLUMN,L)=B(ICOLUMN,L)/PIVOT(I)
380 DO 550 LI=1,N
  IF (LI-ICOLUMN)400,550,400
400 T=A(LI,ICOLUMN)
  A(LI,ICOLUMN)=0.0
  DO 450 L=1,N
450 A(LI,L)=A(LI,L)-A(ICOLUMN,L)*T
  IF(M)530,530,460
460 DO 500 L=1,M
500 B(LI,L)=B(LI,L)-B(ICOLUMN,L)*T
530 CONTINUE
  DO 710 I=1,N
  LN=N+1-I
  IF(INDEX(L,1)-INDEX(L,2))630,710,630
630 JROW=INDEX(L,1)
  JCOLUMN=INDEX(L,2)
  DO 705 K=1,N
  SWAP=A(K,JROW)
```

```
A(K,JROW)=A(K,JCOLUM)
A(K,JCOLUM)=SWAP
705 CONTINUE
710 CONTINUE
740 RETURN
END
```

```

SUBROUTINE PLOTB (NO,N,AA,BB)
SUBROUTINE PLOT B
C
C
A= LARGEST OF FC AND FM, B= SMALLEST
DIMENSION X(116),AA(20),BB(20),Y(4),ABC(2)
COMMON/DATA1/ABC,Y
DATA(ABC=2HNO,3HYES),(Y=1H,1HC,1H*,1HM)
A=AA(1)
B=A
DO 900 I=1,N
IF(AA(I)-A)905,905,910
910 A=AA(I)
905 IF(BB(I)-A)915,915,920
920 A=BB(I)
915 IF(AA(I)-B)930,925,925
930 B=AA(I)
925 IF(BB(I)-B)935,900,900
935 B=BB(I)
900 CONTINUE
FACTOR = 1.0
520 IF (A-B-1000.0) 500, 510, 510
500 A = 2.0*A
B = 2.0*B
FACTOR = 2.0*FACTOR
GO TO 520
510 KD = (A-B)/112.0 + 1.0
KS = IFIX(B) - 2*KD
WRITE (6,1)
1 FORMAT(119H0...0.....1.....2.....3.....4.....
15.....6.....7.....8.....9.....10.....11...)
DO 100 I=1,N
DO 110 K=1,116
110 X(K)=Y(1)
K = AA(I)*FACTOR
K = (K-KS)/KD
X(K) = Y(2)
L = BB(I)*FACTOR
L = (L-KS)/KD
IF(L-K)120,130,120
130 X(L)=Y(3)
GO TO 105
120 X(L)=Y(4)
105 INO=I+NO-1
100 WRITE (6,90)INO,X
90 FORMAT(1X13,116A1)
WRITE (6,1)
RETURN
END

```



```

C      SUBROUTINE JACOBI (N,Q,JVEC,M,V)
C      SUBPROGRAM FOR DIAGONALIZATION OF MATRIX Q BY SUCCESSIVE ROTATIONS
C      DIMENSION Q(4,4),V(4,4),X(4),IH(4)
C
C      NEXT 8 STATEMENTS FOR SETTING INITIAL VALUES OF MATRIX V
C
C      IF(JVEC) 10,15,10
10 DO 14 I=1,N
   DO 14 J=1,N
   IF(I-J) 12,11,12
11 V(I,J)=1.0
   GO TO 14
12 V(I,J)=0.
14 CONTINUE
C
C      15 M=0
C      NEXT 8 STATEMENTS SCAN FOR LARGEST OFF DIAG. ELEM. IN EACH ROW
C      X(I) CONTAINS LARGEST ELEMENT IN ITH ROW
C      IH(I) HOLDS SECOND SUBSCRIPT DEFINING POSITION OF ELEMENT
C
C      MI=N-1
C      DO 30 I=1,MI
C      X(I)=0.
C      MJ=I+1
C      DO 30 J=MJ,N
C      IF (X(I)-ABS (Q(I,J))) 20,20,30
20 X(I)=ABS (Q(I,J))
   IH(I)=J
30 CONTINUE
C
C      NEXT 7 STATEMENTS FIND FOR MAXIMUM OF X(I)S FOR PIVOT ELEMENT
C
C      40 DO 70 I=1,MI
C      IF(I-1) 60,60,45
C      45 IF (XMAX-X(I)) 60,70,70
C      60 XMAX=X(I)
C      IP=I
C      JP=IH(I)
C      70 CONTINUE
C
C      NEXT 2 STATEMENTS TEST FOR XMAX,IF LESS THAN 10**-8,GO TO 1000
C
C      EPSI=1.E-8
C      IF (XMAX-EPSI) 1000,1000,148
C
C      148 M=M+1
C
C      NEXT 11 STATEMENTS FOR COMPUTING TANG,SINE,COSN,Q(I,I),Q(J,J)
C
C      IF (Q(IP,IP)-Q(JP,JP)) 150,151,151
150 TANG =-2.*Q(IP,JP)/(ABS(Q(IP,IP)-Q(JP,JP))+SQRT((Q(IP,IP)-Q(JP,JP)
   )**2+4.*Q(IP,JP)**2))
   GO TO 160
151 TANG =+2.*Q(IP,JP)/(ABS(Q(IP,IP)-Q(JP,JP))+SQRT((Q(IP,IP)-Q(JP,JP)
   )**2+4.*Q(IP,JP)**2))
160 COSN=1.0/SQRT(1.0+TANG**2)
   SINE=TANG*COSN
   QII= Q(IP,IP)
   Q(IP,IP)= COSN**2*(QII+TANG*(2.*Q(IP,JP)+TANG*Q(JP,JP)))
   Q(JP,JP)= COSN**2*(Q(JP,JP)-TANG*(2.*Q(IP,JP)-TANG*QII))

```

Q(IP,JP)=0.

C
C

NEXT 4 STATEMENTS FOR PSEUDO RANK OF THE EIGENVALUES
IF (Q(IP,IP)-Q(JP,JP)) 152,153,153

152 TEMP=Q(IP,IP)
Q(IP,IP)=Q(JP,JP)
Q(JP,JP)=TEMP

C
C
C

NEXT 6 STATEMENTS ADJUST SIN,COS FOR COMPUTATION OF Q(I,K),V(I,K)

IF(SINE) 154,155,155
154 TEMP=+COSN
GO TO 170
155 TEMP=-COSN
170 COSN=ABS(SINE)
SINE=TEMP

C
C
C
C
C

NEXT 10 STATEMENTS FOR INSPECTING THE I'S BETWEEN I+1 AND N-1 TO
DETERMINE WHETHER A NEW MAXIMUM VALUE SHOULD BE COMPUTED SINCE
THE PRESENT MAXIMUM IS IN THE I OR J ROW

153 DO 350 I=1,MI
IF (I-IP) 210,350,200
200 IF (I-JP) 210,350,210
210 IF (IH(I)-IP) 230,240,230
230 IF (IH(I)-JP) 350,240,350
240 K= IH(I)
TEMP=Q(I,K)
Q(I,K)=0.
MJ=I+1
X(I)=0.

C
C
C

NEXT 5 STATEMENTS SEARCH IN DEPLETED ROW FOR NEW MAXIMUM

DO 320 J=MJ,N
IF (X(I)-ABS(Q(I,J))) 300,300,320
300 X(I)=ABS(Q(I,J))
IH(I)=J
320 CONTINUE
Q(I,K)=TEMP
350 CONTINUE

C

X(IP)=0.
X(JP)=0.

C NEXT 30 STATEMENTS FOR CHANGING THE OTHER ELEMENTS OF Q

C DO 530 I=1,N

C IF (I-IP) 370,530,420
370 TEMP=Q(I,IP)
Q(I,IP)=COSN*TEMP+SINE*Q(I,JP)
IF (X(I)-ABS(Q(I,IP))) 380,390,390
380 X(I)=ABS(Q(I,IP))
IH(I)=IP
390 Q(I,JP)=-SINE*TEMP+COSN*Q(I,JP)
IF (X(I)-ABS(Q(I,JP))) 400,530,530
400 X(I)=ABS(Q(I,JP))
IH(I)=JP
GO TO 530

C 420 IF (I-JP) 430,530,480
430 TEMP =Q(IP,I)
Q(IP,I)=COSN*TEMP+SINE*Q(I,JP)
IF (X(IP)-ABS(Q(IP,I))) 440,450,450
440 X(IP)=ABS(Q(IP,I))
IH(IP)=I
450 Q(I,JP)=-SINE*TEMP+COSN*Q(I,JP)
IF (X(I)-ABS(Q(I,JP))) 400,530,530

C 480 TEMP=Q(IP,I)
Q(IP,I)=COSN*TEMP+SINE*Q(JP,I)
IF(X(IP)-ABS(Q(IP,I))) 490,500,500
490 X(IP)=ABS(Q(IP,I))
IH(IP)=I
500 Q(JP,I)=-SINE*TEMP+COSN*Q(JP,I)
IF (X(JP)-ABS(Q(JP,I))) 510,530,530
510 X(JP)=ABS(Q(JP,I))
IH(JP)=I
530 CONTINUE

C C NEXT 6 STATEMENTS TEST FOR COMPUTATION OF EIGENVECTORS

C IF (JVEC) 540,40,540
540 DO 550 I=1,N
TEMP=V(I,IP)
V(I,IP)= COSN*TEMP+SINE*V(I,JP)
550 V(I,JP)=-SINE*TEMP+COSN*V(I,JP)
GO TO 40
1000 RETURN
END

```

SUBROUTINE JACOBI(N,Q,JVEC,M,V)
SUBPROGRAM FOR DIAGONALIZATION OF MATRIX Q BY SUCCESSIVE ROTATIONS
DIMENSION Q(4,4),V(4,4),X(4),IH(4)
13 FORMAT (2E15.5)
C
C
C
NEXT 8 STATEMENTS FOR SETTING INITIAL VALUES OF MATRIX V
C
C
C
IF(JVEC) 10,15,10
10 DO 14 I=1,N
DO 14 J=1,N
IF(I-J) 12,11,12
11 V(I,J)=1.0
GO TO 14
12 V(I,J)=0.
14 CONTINUE
C
15 M=0
NEXT 8 STATEMENTS SCAN FOR LARGEST OFF DIAG. ELEM. IN EACH ROW
X(I) CONTAINS LARGEST ELEMENT IN ITH ROW
IH(I) HOLDS SECOND SUBSCRIPT DEFINING POSITION OF ELEMENT
C
C
C
MI=N-1
DO 30 I=1,MI
X(I)=0.
MJ=I+1
DO 30 J=MJ,N
IF (X(I)-ABS(Q(I,J))) 20,20,30
20 X(I)=ABS(Q(I,J))
IH(I)=J
30 CONTINUE
C
C
NEXT 7 STATEMENTS FIND FOR MAXIMUM OF X(I)S FOR PIVOT ELEMENT
40 DO 70 I=1,MI
IF(I-1) 60,60,45
45 IF (XMAX-X(I)) 60,70,70
60 XMAX=X(I)
IP=I
JP=IH(I)
70 CONTINUE
C
C
NEXT 2 STATEMENTS TEST FOR XMAX, IF LESS THAN 10**-8, GO TO 1000
C
C
EPSI=1./((10.)**16)
IF (XMAX-EPSI) 1000,1000,148
C
148 M=M+1
C
C
NEXT 11 STATEMENTS FOR COMPUTING TANG,SINE,COSN,Q(I,I),Q(J,J)
C
C
IF (Q(IP,IP)-Q(JP,JP)) 150,151,151
150 TANG =-2.*Q(IP,JP)/(ABS(Q(IP,IP)-Q(JP,JP))+SQRT((Q(IP,IP)-Q(JP,JP)
1)**2+4.*Q(IP,JP)**2))
GO TO 160
151 TANG =+2.*Q(IP,JP)/(ABS(Q(IP,IP)-Q(JP,JP))+SQRT((Q(IP,IP)-Q(JP,JP)
1)**2+4.*Q(IP,JP)**2))
160 COSN=1.0/SQRT(1.0+TANG**2)
SINE=TANG*COSN
QII= Q(IP,IP)
Q(IP,IP)= COSN**2*(QII+TANG*(2.*Q(IP,JP)+TANG*Q(JP,JP)))
Q(JP,JP)= COSN**2*(Q(JP,JP)-TANG*(2.*Q(IP,JP)-TANG*QII))

```

Q(IP,JP)=0.

C
C
C
C

NEXT 4 STATEMENTS FOR PSEUDO RANK OF THE EIGENVALUES
IF (Q(IP,IP)-Q(JP,JP)) 152,153,153

152 TEMP=Q(IP,IP)

Q(IP,IP)=Q(JP,JP)

Q(JP,JP)=TEMP

NEXT 6 STATEMENTS ADJUST SIN,COS FOR COMPUTATION OF Q(I,K)*V(I,K)

IF(SINE) 154,155,155

154 TEMP=+COSN

GO TO 170

155 TEMP=-COSN

170 COSN=ABS(SINE)

SINE=TEMP

C
C
C
C

NEXT 10 STATEMENTS FOR INSPECTING THE IHS BETWEEN I+1 AND N-1 TO
DETERMINE WHETHER A NEW MAXIMUM VALUE SHOULD BE COMPUTED SINCE
THE PRESENT MAXIMUM IS IN THE I OR J ROW

153 DO 350 I=1,MI

IF (I-IP) 210,350,200

200 IF (I-JP) 210,350,210

210 IF (IH(I)-IP) 230,240,230

230 IF (IH(I)-JP) 350,240,350

240 K= IH(I)

TEMP=Q(I,K)

Q(I,K)=0.

MJ=I+1

X(I)=0.

C
C
C

NEXT 5 STATEMENTS SEARCH IN DEPLETED ROW FOR NEW MAXIMUM

DO 320 J=MJ,N

IF (X(I)-ABS(Q(I,J))) 300,300,320

300 X(I)=ABS(Q(I,J))

IH(I)=J

320 CONTINUE

Q(I,K)=TEMP

350 CONTINUE

C
C
C

X(IP)=0.

X(JP)=0.

C
C
C

NEXT 30 STATEMENTS FOR CHANGING THE OTHER ELEMENTS OF Q

DO 530 I=1,N

IF (I-IP) 370,530,420

370 TEMP=Q(I,IP)

Q(I,IP)=COSN*TEMP+SINE*Q(I,JP)

IF (X(I)-ABS(Q(I,IP))) 380,390,390

380 X(I)=ABS(Q(I,IP))

IH(I)=IP

390 Q(I,JP)=-SINE*TEMP+COSN*Q(I,JP)

IF (X(I)-ABS(Q(I,JP))) 400,530,530

400 X(I)=ABS(Q(I,JP))

IH(I)=JP

GO TO 530

```
420 IF (I=JP) 430,530,440  
430 TEMP=Q(IP,I)  
Q(IP,I)=COSN*TEMP+SINE*Q(I,JP)  
IF (X(IP)-ABS(Q(IP,I))) 440,450,450  
440 X(IP)=ABS(Q(IP,I))  
IH(IP)=I  
450 Q(I,JP)=-SINE*TEMP+COSN*Q(I,JP)  
IF (X(I)-ABS(Q(I,JP))) 400,530,530
```

```
C  
480 TEMP=Q(IP,I)  
Q(IP,I)=COSN*TEMP+SINE*Q(JP,I)  
IF (X(IP)-ABS(Q(IP,I))) 490,500,500  
490 X(IP)=ABS(Q(IP,I))  
IH(IP)=I  
500 Q(JP,I)=-SINE*TEMP+COSN*Q(JP,I)  
IF (X(JP)-ABS(Q(JP,I))) 510,530,530  
510 X(JP)=ABS(Q(JP,I))  
IH(JP)=I  
530 CONTINUE
```

999

NEXT 6 STATEMENTS TEST FOR COMPUTATION OF EIGENVECTORS

```
IF (JVEC) 540,40,540  
540 DO 550 I=1,N  
TEMP=V(I,IP)  
V(I,IP)=COSN*TEMP+SINE*V(I,JP)  
550 V(I,JP)=-SINE*TEMP+COSN*V(I,JP)  
GO TO 40  
1000 AAM=FLOAT(M)  
WRITE (6,13) EPSI,AAM  
RETURN  
END
```

BIBLIOGRAPHY

1. E. Zavoisky, J. Phys. (U.S.S.R.), 41, 211 (1945).
2. B. Bleaney and R.P. Penrose, Nature, 157, 339 (1946).
3. J.M. Daniels and H. Wesemeyer, Can. J. of Phys., 36, 143 (1958).
4. E.G. Brock, D. Stirpe, and E.I. Normata, J. Chem. Phys., 37 2735 (1962).
5. R.W. Schwartz and R.L. Carlin, J. Am. Chem. Soc., 18, 6763 (1970).
6. G. Burns, Phys. Rev., 123, 1634 (1961).
7. A.N. Holden, B.T. Matthias, W.J. Merz, and J.P. Remaka, Phys. Rev., 98, 546 (1955).
8. A.N. Holden, W.J. Merz, J.R. Remaka, and B.T. Matthias, Phys. Rev., 101, 962 (1956).
9. G.S. Bogle, J.R. Gabriel, and G.A. Bottomley, Trans. Faraday Soc., 53, 1058 (1957).
10. J.E. Nertz and J.R. Bolton, Electron Spin Resonance, McGraw-Hill, New-York (1972).
11. G.P. Poole, Electron Spin Resonance, John Wiley & Sons, New-York (1967).
12. A. Abragam and B. Bleaney, Electron Paramagnetic Resonance of Transition Ions, Clarendon Press, Oxford (1970).
13. G. Baym, Lectures on Quantum Mechanics, Benjamin, New-York (1969).

14. S.K. Miera and G.R. Sharp, Jour. Mag. Res., (In Press).
15. S.K. Miera, Jour. Mag. Res., (In Press).
16. S. Geller and D.P. Booth, Z. Krist., 111, 2 (1958).
17. S. Geller, Z. Krist., 114, 148 (1960).
18. B.J.B. Schein, E.C. Lingafelter, and J.M. Stewart, J. Chem. Phys., 47, 5183 (1967).
19. G.R. Sharp, Thesis, Sept. 1972. Sir George Williams University.